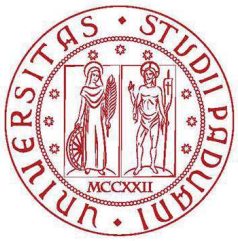

UNIVERSITÀ DEGLI STUDI DI PADOVA

Dipartimento di Fisica e Astronomia "Galileo Galilei"

Master Degree in Physics

Final Dissertation

Allometric scaling in biological and ecological systems

Thesis supervisor

Prof. Amos Maritan

Candidate

Davide Marcato

Academic Year 2020/2021

Contents

Introduction

The study of the phenomenon generally known as "life" is maybe one of the most difficult challenges Science has to tackle. The arduousness stems primarily from the impressive diversity and complexity of living systems, which seem to retain the possibility of formulating universal theories such as the ones known in Physics. This is probably the reason underlying the fact that Biology has proceeded for many years following a one-at-a-time approach ([19]), which brought to the knowledge of myriads of life essential components (especially from a biochemical perspective), but without succeeding in explaining emergent properties of living systems.

In the past century a new strategy has taken hold, which consists in looking at complex biological and ecological systems from a wider point of view, neglecting the individual details of the various components but rather concentrating on integral aspects. From this side, physicists have played an important role: the application of Statistical Mechanics and other concepts from Physics have been applied to Life Sciences, allowing the construction of models with a mathematical back-bone for the study of life at several scales, from protein folding to ecosystem organization.

A topic that has received particular attention in the past two decades from the Physics community is that of *allometry*. This term was coined in 1936 by Huxley and Teissier ([12]) to indicate the relative growth of the parts with respect to the whole or, more generally, proportions in living organisms. The interest probably stemmed from the fact that, despite the diversity and complexity mentioned before, empirical findings have revealed that the scaling of some quantities with body size seems to obey some simple rules which could be deemed as universal. As a matter of fact, in the same paper from 1936 Huxley and Teissier propose the *"elementary law of relative growth or law of simple allometry"* which establishes that for some mass-dependent biological variable Y, being M the whole-body mass, there exists

a power law relation of the kind

$$Y = Y_0 M^b$$

where Y_0 is a proportionality constant and b is called *allometric exponent*. This allometric law captures a simple pattern that was observed in the previous years for instance in the study of the relation of brain size ([11]) and metabolic rate ([14]) with body mass. Throughout the years, an increasing number of quantities obeying the law of simple allometry has been found: the large amount of data collected allowed to determine the values of the allometric exponents and to test for their universality. A very intriguing discovery was that the allometric exponents were usually found to be simple multiples of 1/4, a fact for which no explanation was found for several decades. Despite the vast amount of empirical confirmations, it is only in 1997 that a first theoretical model by West, Brown and Enquist ([23]) was proposed to provide an exhaustive explanation on the reasons why some allometric relations are as they are. The model was very influential and gives predictions in good accord with empirical data, as can be seen in Figure 1.

Cardiovascular			Respiratory		
Variable	Exponent		Variable	Exponent	
	Predicted	Observed		Predicted	Observed
Aorta radius r_0	3/8 = 0.375	0.36	Tracheal radius	3/8 = 0.375	0.39
Aorta pressure Δp_0	0 = 0.00	0.032	Interpleural pressure	0 = 0.00	0.004
Aorta blood velocity u_0	0 = 0.00	0.07	Air velocity in trachea	0 = 0.00	0.02
Blood volume V_b	1 = 1.00	1.00	Lung volume	1 = 1.00	1.05
Circulation time	1/4 = 0.25	0.25	Volume flow to lung	3/4 = 0.75	0.80
Circulation distance l	1/4 = 0.25	ND	Volume of alveolus V_A	1/4 = 0.25	ND
Cardiac stroke volume	1 = 1.00	1.03	Tidal volume	1 = 1.00	1.041
Cardiac frequency ω	−1/4 = −0.25	−0.25	Respiratory frequency	−1/4 = −0.25	−0.26
Cardiac output E	3/4 = 0.75	0.74	Power dissipated	3/4 = 0.75	0.78
Number of capillaries N_c	3/4 = 0.75	ND	Number of alveoli N_A	3/4 = 0.75	ND
Service volume radius	1/12 = 0.083	ND	Radius of alveolus r_A	1/12 = 0.083	0.13
Womersley number α	1/4 = 0.25	0.25	Area of alveolus A_A	1/6 = 0.083	ND
Density of capillaries	−1/12 = −0.083	−0.095	Area of lung A_L	11/12 = 0.92	0.95
O_2 affinity of blood P_{50}	−1/12 = −0.083	−0.089	O_2 diffusing capacity	1 = 1.00	0.99
Total resistance Z	−3/4 = −0.75	−0.76	Total resistance	−3/4 = −0.75	−0.70
Metabolic rate B	3/4 = 0.75	0.75	O_2 consumption rate	3/4 = 0.75	0.76

Figure 1: Values of the allometric exponents predicted by the WBE (West, Brown and Enquist) model compared with experimental measurements. Figure from [23].

However, WBE model was not universally accepted because of the lack of strictness and the stringent hypotheses. Other ideas have been put forward since then, but the true origin of allometric quarter-power scaling is still a matter of debate.

The aim of this work is to present the concept of allometric scaling from a mainly theoretical point of view and to explore the possible applications to the modeling of biological and ecological systems.
The first chapter deals with maybe the most famous example of allometric scaling, i.e. Kleiber's law, which describes the basal metabolic rate as a function of body mass. Some consequences of this universal relation will be explored, both at the level of single individuals and entire ecosystems, highlighting the central importance of energetic constraints in the structure of life.
In Chapter 2, the ideas of allometry and metabolic optimization, together with physical concepts such as power law distributions in critical phenomena and finite-size scaling, will be exploited in order to model forest communities. For instance, it will be shown how one could estimate the distribution of tree heights or tree diameters in a forest covering a certain area.
Chapter 3 is concerned with an application of allometric scaling as a theoretical framework for designing particular *in vitro* systems that go under the name of *body-on-a-chip*. The model presented in [1] will be analyzed and discussed in detail. Also, some of the basic assumptions will be modified, and the new results will be compared to the ones of the original model.

Chapter 1

Metabolic theory

Several biological variables (e.g. life spans, metabolic rates, biomass production rate) depend on body size. It has been known for almost a century that this dependency can typically be expressed in the form of a power law

$$Y \sim M^b \tag{1.1}$$

where Y indicates the biological variable of interest, M is body mass and b is called the *allometric exponent*. This is known as *allometric scaling*. The allometric exponent b is characteristic of a particular quantity Y. Despite the range of body masses of living organisms extends for over 20 orders of magnitude, b is empirically observed to be scale invariant: a biological quantity Y scales following roughly the same allometric relation from unicellular organisms, to insects, to amphibians, to mammals.

In this chapter a particular biological variable will be taken into consideration, i.e. the metabolic rate, and its central importance in ecology will be highlighted.

1.1 Kleiber's law

All living organisms continuously take up resources from the environment they live in, consume those resources within their bodies in order to obtain energy for various biological activities and excrete altered forms of materials and energy back into the environment. This processing of resources is called *metabolism* ([6]). The rate at which the processes that constitute metabolism occur is called the *metabolic rate*. From a more physical point of view,

metabolic rate can be defined as the energy consumed by an organism per unit time, and it has therefore the dimensions of power. A more precise definition distinguishes between

- Basal metabolic rate: the minimal rate of energy expenditure for an organism at rest in ideal conditions;
- Field metabolic rate: the rate of energy expenditure of a free-living organism, which includes allocation to various tasks such as growth, reproduction and foraging;
- Maximal metabolic rate: rate of energy consumption of an organism during a maximal sustained activity.

Henceforth, all the considerations about metabolic rate will implicitly refer to *basal* metabolic rate (unless otherwise stated), which will be denoted with B. Given the astounding diversity between organisms in terms of internal functioning and structure, it would be seemingly hopeless to search for simple and general patterns in the behavior of B. Actually, as empirical data show, this is not the case.

The first question to be addressed is: what does B depend on? It is certainly reasonable to assume that organisms of different sizes will consume different amounts of energy per unit time: hence, the metabolic rate B has to depend on the size of an organism, i.e. its volume. Actually, living organisms can be considered to have a roughly constant density, very close to the density of water. Therefore B can be thought to depend on the organism's mass M rather than on its volume. The most immediate guess could be that B is simply proportional to M: an organism which is 10 times heavier than another one has 10 times more cells to nourish, and it will therefore need 10 times more energy per unit time. Actually, in 1932, Swiss biologist Max Kleiber showed empirically that this is not the case ([14]): B scales sublinearly with body mass, following a power law with an exponent close to 3/4

$$B \sim M^{3/4} \tag{1.2}$$

This is maybe the most famous example of allometric scaling and it is known as *Kleiber's law*. Aside from small deviations of the allometric exponent from the value of 3/4, Kleiber's law has been widely tested and was

observed to hold true for all living organisms, from bacteria to big mammals and trees.

A less intuitive observation is that B should exhibit a dependence also on temperature T. This is because, from a microscopical point of view, metabolism is based on a series of biochemical reactions. The number of reactions that constitute metabolism in all various types of organisms is bewildering, as well as the number of enzymes and substrates that participate. However, the fundamental biochemistry is common to the vast majority of organisms ([6]): heterotrophs[1]obtain energy through respiration, based on the reaction

$$CH_2O + O_2 \longrightarrow \text{energy} + CO_2 + H_2O$$

which is then exploited by cells. Autotrophs[1] use instead the inverse reaction in the process of photosynthesis, where energy is provided by photons. As it is known, every chemical reaction possesses an activation energy. Increasing the absolute temperature T results in an increase of the proportion of molecules with enough kinetic energy to overcome the activation potential barrier, and thus the reaction rate. This proportion of molecules is given by the Boltzmann factor

$$e^{-E/k_BT} \tag{1.3}$$

where k_B is the Boltzmann constant and E is the average activation energy of the fundamental reactions of metabolism. It has to be mentioned, however, that these considerations are valid only in a limited range of temperatures, namely from 0 °C to about 40 °C ([8]). By combining this result with Kleiber's law, one can estimate the dependence of metabolic rate B upon the organism mass M and temperature T ([8])

$$B = B_0 M^{3/4} e^{-E/k_BT} \tag{1.4}$$

The proportionality constant B_0 is characteristic of a particular group. What does this equation tell us? Let M_1 and M_2 be the masses of organisms of the same group (e.g. mammals) that operate at the same body temperature. If, say, $M_2/M_1 = 10$, then $B_2/B_1 \simeq 5.6$: despite being 10 times larger,

[1]Heterotrophs are organisms which rely on the intake from external resources of organic carbon. Autotrophs instead exploit energy from sunlight to convert inorganic carbon dioxide to organic carbon compounds.

organism 2 consumes only 5.6 times more energy per unit time with respect to organism 1. The knowledge of the behavior of B is of fundamental importance since *"much of the variation among ecosystems, including their biological structures, chemical compositions, energy and material fluxes, population processes, and species diversities, depends on the metabolic characteristics of the organisms that are present"* ([6]).

It's worth verifying how well equation 1.4 fits experimental data for different groups. It is possible to rearrange equation 1.4 in order to *mass-correct* the metabolic rate, i.e.

$$BM^{-3/4} = B_0 e^{-E/k_B T} \tag{1.5}$$

By taking the logarithm of both sides one obtains

$$\ln(BM^{-3/4}) = -\frac{E}{k_B T} + C \tag{1.6}$$

where $C = \ln B_0$ is a constant that does not depend neither on M nor on T.

Equation 1.6 predicts that there should be a linear relation between the logarithm of the mass-corrected metabolic rate and $1/k_B T$: the slope of the straight line should give the average activation energy for the biochemical reactions that constitute metabolism. In principle, different taxonomic groups (e.g. unicellular organisms, plants, fish, mammals and birds) could be characterized by different values of E and C. However, since the biochemical reactions of metabolism are basically the same for all organisms, the various fits for different groups should yield straight lines with similar slopes. Moreover, activation energies of metabolic biochemical reactions are known to vary from 0.2 to 1.2 eV, with an average of approximately 0.6 eV: these are the expected values of the slopes ([8]).

As shown in Figure 1.1, all the predictions are verified by experimental data. In particular, it is evident that the slopes of the various straight lines are very similar to one another, and the average slope is 0.69 eV, close to the predicted value of 0.6 eV. Equation 1.4 can be rearranged in the following fashion

$$\ln(Be^{E/k_B T}) = \frac{3}{4}\ln(M) + C \tag{1.7}$$

This equation predicts a linear relation (in a log-log plot) between body mass M and the *temperature-corrected metabolic rate*, with a slope close to

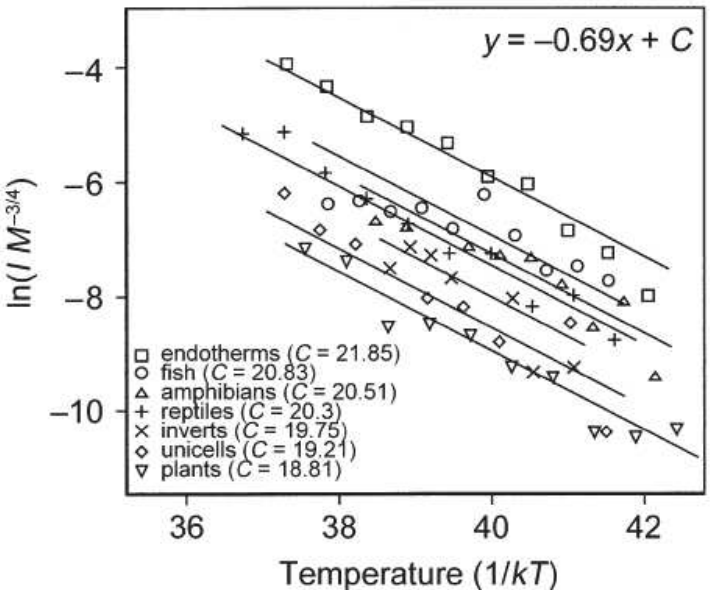

Figure 1.1: Mass-corrected metabolic rate (here metabolic rate is denoted with I) as a function of the inverse temperature for different taxonomic groups (listed in the figure). The quantity $1/k_BT$ is measured in eV^{-1}. Mass-corrected metabolic rate is measured in $\mathrm{W/g}^{3/4}$. Figure from [6].

3/4. The value of C should be similar to the one found with equation 1.6. Figure 1.2 shows that these predictions are verified.

It is worth noting how equation 1.4 provides predictions in good accord with experimental data for an impressive range of values of M, from small unicellular organisms to big mammals.

1.2 Consequences for life

In the following, some predictions about different aspects of an organism's life based on equation 1.4 are presented. The first two deal with the level of a single individual, whereas the third refers to a whole population.

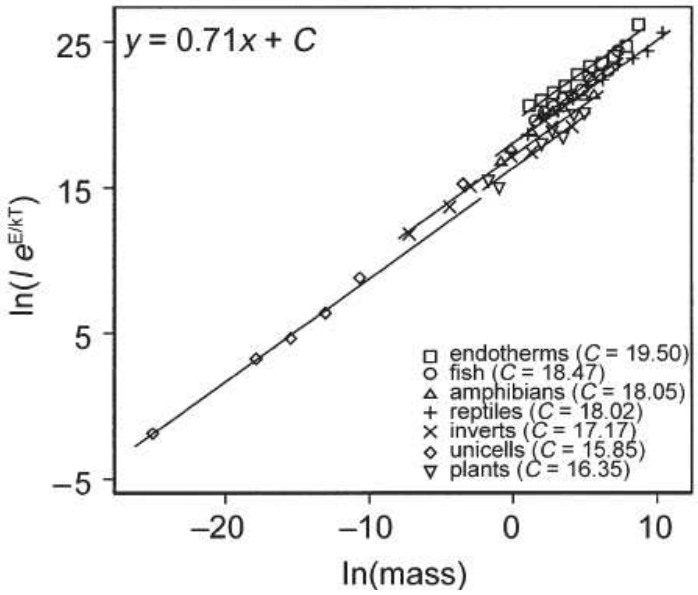

Figure 1.2: Temperature-corrected metabolic rate (here metabolic rate is denoted with I, measured in W) as a function of body mass M (in grams). Figure from [6].

1.2.1 Ontogenetic growth

During growth, the energy produced through metabolism within an organism has to be allocated in maintenance of existing tissue and biomass production. Therefore, one can assume ([24]) that the total energy consumed per unit time is the sum of two contributions, namely

$$B(t) = B_c N_c(t) + E_c \frac{dN_c(t)}{dt} \tag{1.8}$$

where B_c is the metabolic rate of a single cell, N_c is the total number of cells in the organism and E_c is the energy required to create a new cell. Notice that metabolic rate B has a time dependence due to the variation of the number of cells. A more precise version of the previous equation takes into account also the differences between different types of cells: here, following [24], we're considering an "average" cell. We denote with $m(t)$ the mass of an organism at time t: indeed $m(t) = N_c(t)m_c$, where m_c is the mass of a single cell. Thus the equation can be rewritten as

$$\frac{dm(t)}{dt} = \frac{m_c}{E_c}B(t) - \frac{B_c}{m_c}m(t) \tag{1.9}$$

and, by using equation 1.4 for B

$$\frac{dm(t)}{dt} = a(T)m^{3/4}(t) - bm(t) \tag{1.10}$$

where $a(T) = m_c B_0 e^{-E/k_B T}/E_c$ and $b = B_c/E_c$. Organisms begin their life with a certain mass m_0 at time $t = 0$ and eventually stop growing when they reach maturity, asymptotically approaching mass M. Note that we're assuming that temperature T does not vary with time. The value of M is given by

$$\frac{dm(t)}{dt} = 0 \implies a(T)M^{3/4} = bM \implies M = \left(\frac{a(T)}{b}\right)^4 \tag{1.11}$$

Therefore we can write

$$\frac{dm(t)}{dt} = a(T)m^{3/4}(t)\left[1 - \left(\frac{m(t)}{M}\right)^{1/4}\right] \tag{1.12}$$

At this point we can introduce the quantity $x(t) = (m(t)/M)^{1/4}$. With this substitution we obtain

$$\frac{dx(t)}{dt} = \frac{a(T)}{4}M^{-1/4}[1 - x(t)] \tag{1.13}$$

which can be easily solved by separation of variables and yields, remembering the definition of $x(t)$ and the initial condition $m(0) = m_0$

$$\left(\frac{m(t)}{M}\right)^{1/4} = 1 - \left[1 - \left(\frac{m_0}{M}\right)^{1/4}\right]e^{-\frac{a(T)}{4M^{1/4}}t} \tag{1.14}$$

This is the complete solution of equation 1.12, which well-fits experimental data for different groups of organisms (as shown in [24], even though the temperature dependence is not considered there). Also, if one defines the dimensionless mass ratio $r = (m(t)/M)^{1/4}$ and the dimensionless time $\tau = at/4M^{1/4} - \ln[1 - (m_0/M)^{1/4}]$, then the data of all species should collapse on the universal curve defined by $r = 1 - e^{-\tau}$; this collapse is actually observed, as reported in Figure 1.3.

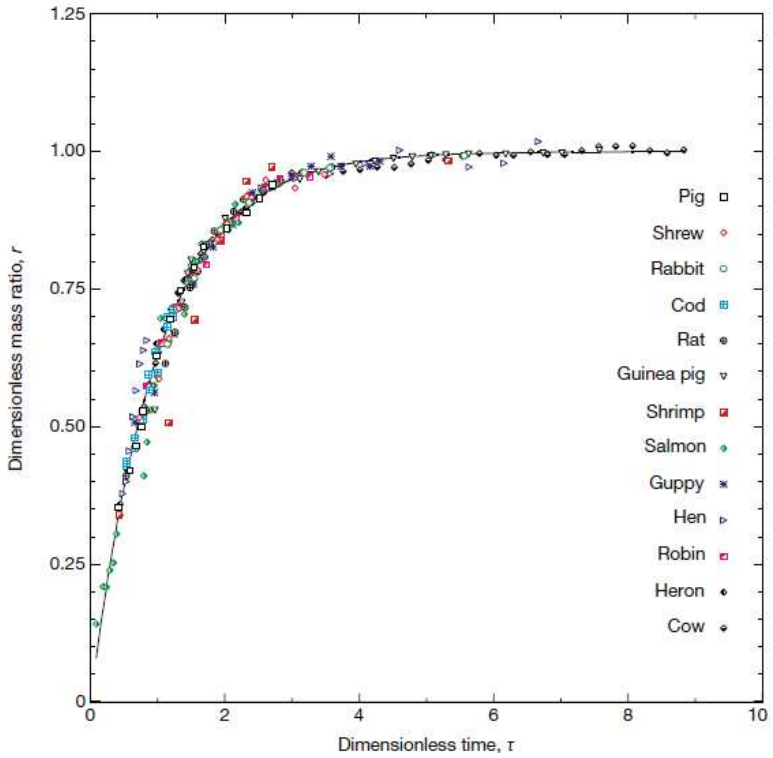

Figure 1.3: Data on the growth of individuals of different species were expressed in terms of r and τ and plotted. The collapse on the curve defined by $r = 1 - e^{-\tau}$ is apparent. Figure from [24].

If we focus on a particularly short period of time, such that $m(t) \ll M$ throughout the whole period and $m_0 \simeq 0$, equation 1.12 is approximated by

$$\frac{dm(t)}{dt} = a(T)m^{3/4}(t) \implies \frac{m^{1/4}(t)}{t} = \frac{a(T)}{4} \tag{1.15}$$

This is for example a good approximation for the description of embryonic development. By recalling the definition of $a(T)$ one obtains

$$\log\left(\frac{m^{1/4}(t)}{t}\right) = -\frac{E}{k_B T} + \text{const} \tag{1.16}$$

As can be seen in Figure 1.4, this prediction about the temperature dependence of developmental rate is in accord with experimental data. Also,

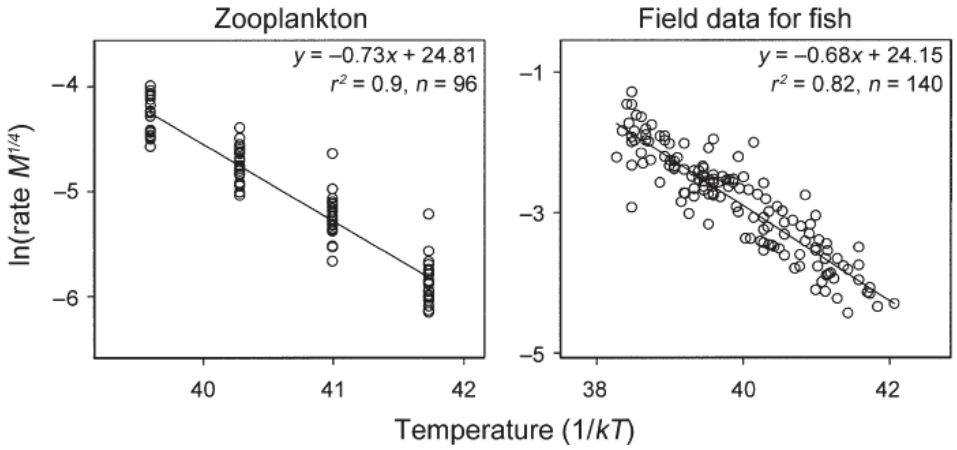

Figure 1.4: Temperature dependence of mass-corrected developmental rates for eggs of zooplankton in laboratory and fish in the field. The developmental rate is equal to the inverse of the hatching time, and it is measured in 1/day. Masses (at hatching) are measured in grams. The quantity $1/k_BT$ is measured in eV^{-1}. Figure from [6].

the slopes of the straight lines are close to the expected value of the average activation energy. It is possible also to rearrange the terms in equation 1.15 to obtain the mass dependence of temperature-corrected developmental rates

$$\log\left(\frac{1}{t}e^{E/k_BT}\right) = -\frac{1}{4}\log(m(t)) + \text{const} \tag{1.17}$$

This prediction is also verified by empirical data, as can be seen in Figure 1.5. The two values obtained for the slopes of the straight lines bracket the expected value of -0.25. These data however refer to embryonic growth, a life stage for which the approximation $m \ll M$ does not lead to significant errors. The same procedure can be repeated also for post-embryonic growth, but in this case the mass correction should be carried out more carefully by using equation 1.12. The results, however, do not change significantly ([9]).

1.2.2 Biological times

Exploiting equation 1.12, it is possible to obtain some predictions about the scaling behavior of lifespans. Let's denote with t_m the time it takes an

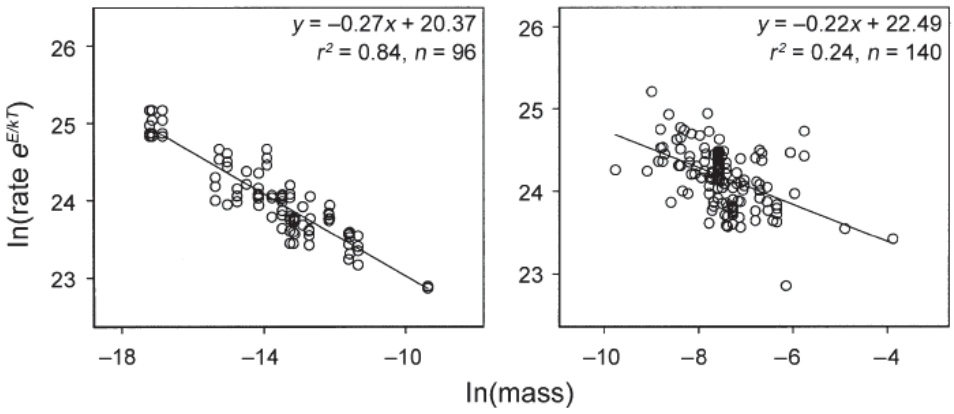

Figure 1.5: Mass dependence of temperature-corrected developmental rates for eggs of zooplankton in laboratory and fish in the field. The developmental rate is equal to the inverse of the hatching time, and it is measured in 1/day. Masses (at hatching) are measured in grams. Figure from [6].

organism to reach a mass $m = (1-\epsilon)M$, where ϵ is a small positive adimensional parameter. The left-hand side of equation 1.12 can be approximated as follows

$$\left(\frac{m}{M}\right)^{1/4} = (1-\epsilon)^{1/4} \simeq 1 - \frac{\epsilon}{4} \tag{1.18}$$

Within this approximation, one finds

$$t_m = \frac{4M^{1/4}}{a(T)} \log\left[\frac{4}{\epsilon}\left(1 - \left(\frac{m_0}{M}\right)^{1/4}\right)\right] \tag{1.19}$$

Ignoring the slowly varying logarithmic contribution, one obtains

$$t_m \sim M^{1/4} e^{E/k_B T} \tag{1.20}$$

This is the time it takes for an organism to grow almost completely. It can be thought of as a characteristic timescale for example for the age at first reproduction or for lifespan. Actually, equation 1.20 is an example of a more general observed pattern, namely that biological times scale as the inverse of the metabolic rate per unit mass. The scaling behavior of lifespans predicted by equation 1.20 is actually confirmed by empirical data ([8]).

1.2.3 Damuth's law

Equation 1.4 leads to consequences which are not limited at the level of single individuals. The fact that organisms of different sizes consume energy at different rates has a remarkable impact in the structure of ecosystems. As an example, let's look at the population density. Based on Verhlust model, the number of individuals in a population as a function of time is described by the differential equation

$$\frac{dN(t)}{dt} = rN(t)\left(1 - \frac{N(t)}{K}\right) \tag{1.21}$$

which solution is the famous logistic curve. This equation predicts that, after an initial stage during which the population grows exponentially, the number of individuals will approach an equilibrium value K, known as *carrying capacity*. The value of K is related to finite resources availability within the environment the population resides in. If we call R the rate of resources supply, one can assume

$$R \sim K \cdot B \tag{1.22}$$

where B is the metabolic rate of a single individual, and, as we know, it is a function of its body mass and temperature. We're considering a one-species population, in which all individuals are identical, in the sense that they're all characterized by the same mass M and temperature T, or that suitable averaging is used. Also, all individuals exploit the same type of resources. By using equation 1.4 one obtains ([6])

$$K \sim RM^{-3/4}e^{E/k_BT} \tag{1.23}$$

The further assumption that R scales linearly with the area A occupied by the population leads to

$$\frac{K}{A} \sim M^{-3/4}e^{E/k_BT} \tag{1.24}$$

Therefore population density is expected to scale as the inverse of B. Despite the simplistic hypothesis, experimental data display the behavior predicted by equation 1.24 (Figure 1.6).

This is a temperature-adjusted version of the so-called Damuth's law ([7]), formulated for the first time in 1981. The temperature correction is

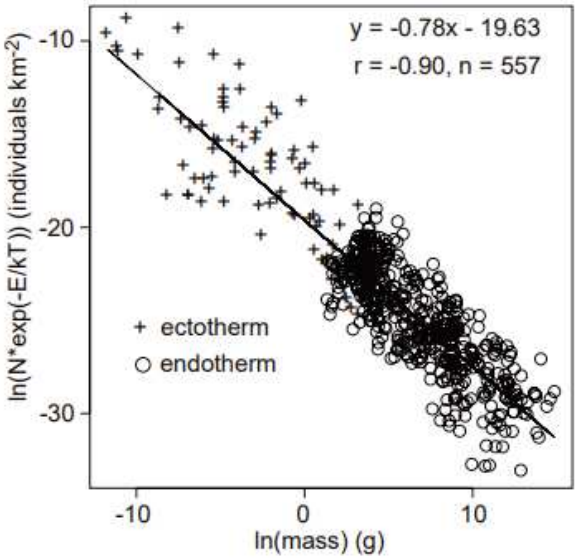

Figure 1.6: Temperature-corrected population density as a function of body mass for both ectotherms and endotherms. Figure from [2].

particularly significant when dealing with ectotherms[2], because temperature gradients (latitudinal or elevational) can have large influence on internal body temperature, and thus on metabolic rate. Qualitatively, the effects of R and M on K/A are not surprising. K/A is a increasing function of R and a decreasing function of M. The temperature dependence, however, might not be so easy to justify. The point is that by increasing the temperature, organisms flux resources through their bodies at a higher rate. Therefore, for a fixed resource supply rate R, less organisms can be sustained: the carrying capacity per unit area lowers.

1.3 Considerations

Despite the astounding diversity of living organisms' phenotypic traits and the complexity of their internal functioning, Kleiber's law seems to capture

[2]Ectotherms are organisms which rely on external sources of heat to control body temperature (e.g. reptiles). Endotherms instead exploit heat produced by their internal functions (e.g. mammals).

a general trend which is obeyed at all scales. This led to the idea that there must be some underlying structure that is common to all organisms, which needs to be understood in order to give Kleiber's law (and other allometric scaling relations) a theoretical foundation. If the temperature dependence in equation 1.4 has a simple explanation in terms of biochemical kinetics (see section 1.1), the mass dependence has proven more challenging to be justified: why is that B scales sublinearly with body mass, and with an exponent close to 3/4?

In the last two decades, there have been some attempts to propose theoretical models which could provide an explanation for Kleiber's law and its universality. The first of these attempts dates back to 1997, when West, Brown and Enquist argued that Kleiber's law is a consequence of the fractal-like structure of nutrients distribution networks in living organisms ([23]). The model, albeit very influential, is not self-consistent ([15]) and relies on quite detailed assumptions about the geometric structure and regularity of the distribution network. As a matter of fact, in 1999 Banavar, Maritan and Rinaldo proposed a new model which also explains Kleiber's law but in a more natural way, as an issue of efficient distribution from a central source in a directed network ([4]), leading to the conclusion that fractality is not the deepest underlying reason for the 3/4 power scaling of metabolic rate. A more recent model ([5]) instead focuses on the surface-volume relation and on the velocity of nutrients. To this day, however, the true origin of Kleiber's law is still debated.

Equation 1.4 offers a basis for numerous applications. Based on considerations on metabolism, it is possible to make predictions about entire ecosystems. Damuth's law, which has been presented in the previous section, is only one of many examples. For instance, it is possible to develop models that describe the structure of forests in terms of height and trunk diameter distribution ([21], see Chapter 2), or the dynamics of trophic levels ([6]), or the species richness in a given environment as shown in Figure 1.7 ([2], [26]). The linkage between individual metabolic performances described by equation 1.4 and ecosystem variables is the pivotal point of the so called *Metabolic Theory of Ecology* ([6]). It has to be mentioned that experimental data often display significant individual variations with respect to the predictions, as can be noted in the various figures presented in this chapter. This may be due to the enormous complexity of ecosystems and their extreme variability shaped by evolution. Nevertheless, the strength of Metabolic Theory may be thought to reside not in its accuracy, but in the strikingly large range of body

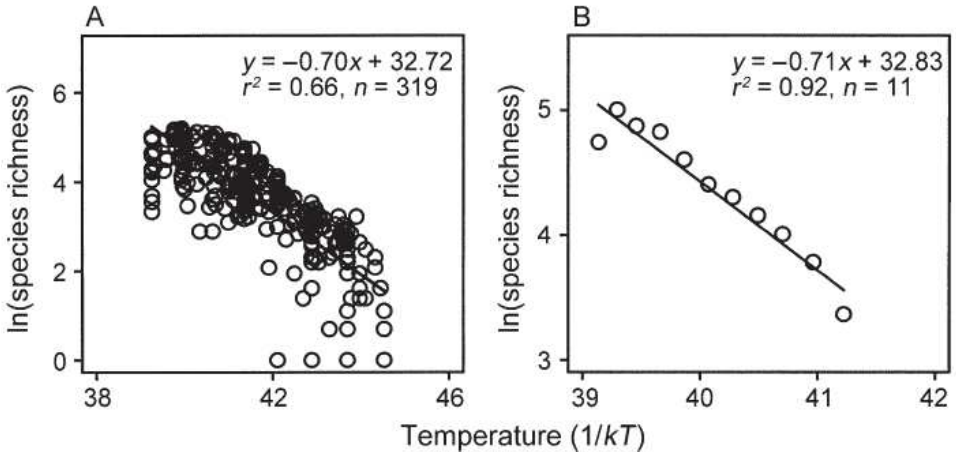

Figure 1.7: Temperature dependence of ectotherms (amphibian) species richness. The quantity $1/k_BT$ is measured in eV^{-1}. The values of the slope are very close to the average activation energy of metabolic reactions. Figure from [2].

masses and temperatures for which it holds true. Individual variations may have to be studied case by case, but the emergent patterns observed empirically suggest that ecosystem structure is largely a consequence of energetic constraints at the level of single individuals.

Chapter 2

Forest structure

In this chapter, the problem of describing and predicting emergent patterns in forest structure is presented. First, a brief discussion about power law distributions and their ubiquitous occurrence in nature is given. Also, the relation between power laws and criticality in living systems will be explored. After that, we'll present a recent model ([21]) which, starting from considerations about the metabolic efficiency of trees and finite-size scaling, offers predictions regarding the distributions of several quantities in steady-state forests. A comparison between theoretical predictions and experimental data is also provided.

2.1 Power law distributions

Figure 2.1 shows the distribution of the heights of American males and of the speed of cars on UK motorways. The two histograms share an important feature: they're (more or less sharply) peaked around a central value, but the curve rapidly decays to zero when one considers larger and larger deviations. This is not a surprising result, since both the heights of humans and the speed of cars on motorways are quantities endowed with a typical *scale*. For example, the typical height of a human being is around 180 cm. There are of course deviations: it is not difficult to find people who are 160 cm or 200 cm tall. However, one can safely state that there are no 5 cm or 500 cm tall people. The same observations holds for the speed of cars on motorways: one typically finds cars which travel at 70 mph. There can be slower or faster ones, but it would very hard to observe cars traveling at, say, 1 or 500 mph.

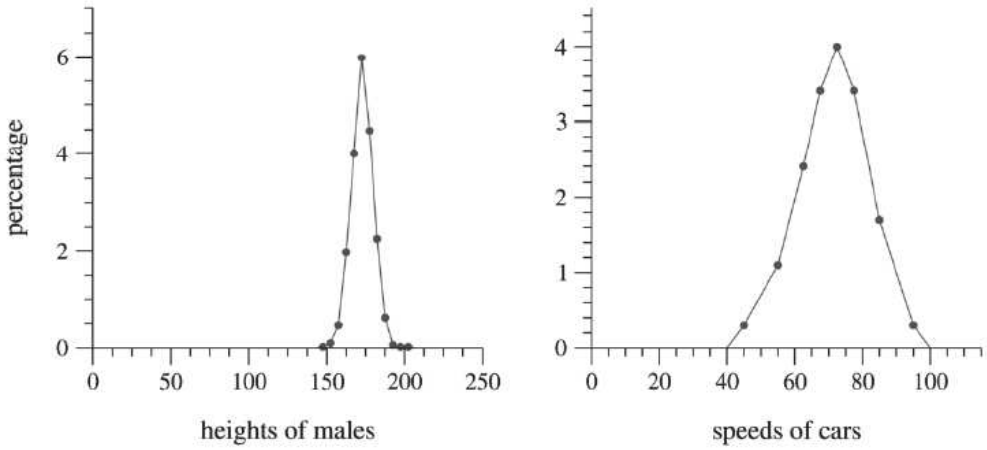

Figure 2.1: The left panel shows the histogram of the height of American males measured in cm, whereas the right panel shows the histogram of the speed of cars on UK motorways, measured in miles/hour. Figure from [20].

There are however quantities which do not possess a typical scale. An example would be the population of cities: it's quite challenging to try to assign a value for the population of a city which could be considered "typical", since this quantity can vary spanning 6 orders of magnitude (from tens to tens of millions). As a matter of fact, the left panel of Figure 2.2 shows how different the histogram for city populations is with respect to the ones presented in Figure 2.1: besides the absence of a central tendency, an apparent feature is the presence of a long tail on the right, which continues for several orders of magnitude. The right panel is maybe more enlightening, since it shows that there exists a roughly linear relation between the logarithm of the distribution and the logarithm of the city population. This means that the distribution follows a *power law*, i.e.

$$p(x) = Cx^{-\alpha} \tag{2.1}$$

where C is a constant that ensures that the distribution is normalized, and $\alpha > 0$.

The case of city populations is just one among many examples of quantities that exhibit a power law distribution: these are observed in a wide variety of contexts belonging to extremely diverse fields. For instance, the frequency of word usage in any human language, the number of citations

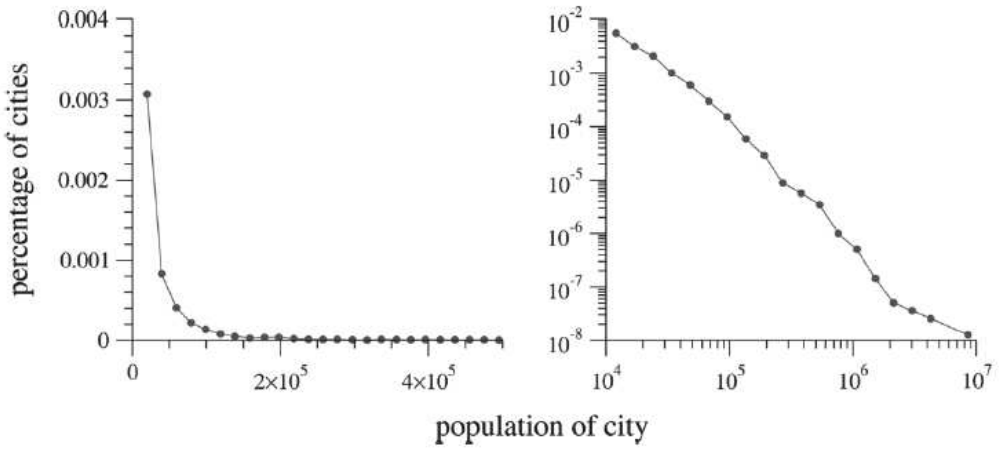

Figure 2.2: The left panel shows the histogram of all US cities with a population greater or equal than 10^4. On the right, the same histogram in a log-log plot. Figure from [20].

received by papers, the number of species in biological taxa, the dimensions of computer files were all noted to be distributed according to a power law ([20]).

2.1.1 Scale invariance

As explained earlier, all the quantities listed above, which distributions follow a power law, are characterized by the fact that they lack a typical scale. This feature is reflected in the functional form of the distribution: actually, power laws are the only distributions which are *scale free*. A distribution $p(x)$ is said to be scale-free if ([19], [20])

$$p(bx) = g(b)p(x) \tag{2.2}$$

i.e. a rescaling of the variable by any factor does not alter the functional form of the distribution, except for a multiplicative term which depends only on the rescaling factor b. This has the immediate consequence that, for any $b \in \mathbb{R}_{>0}$, the ratio

$$\frac{p(bx)}{p(x)} = g(b) \tag{2.3}$$

is independent of x. It is straightforward to verify that a power law satisfies the criterion 2.2. Also, it can be proven that if a function satisfies 2.2, then it must be a power law. Indeed, for $x = 1$ one has

$$p(b) = g(b)p(1) \implies p(bx) = \frac{p(b)p(x)}{p(1)} \tag{2.4}$$

Differentiating both sides with respect to b leads to

$$xp'(bx) = \frac{p(x)}{p(1)}p'(b) \tag{2.5}$$

For $b = 1$ one obtains

$$xp'(x) = \frac{p'(1)}{p(1)}p(x) \tag{2.6}$$

This is a first order differential equation for $p(x)$ which can be solved by separation of variables and yields

$$\ln p(x) = \frac{p'(1)}{p(1)} \ln x + \text{const} \tag{2.7}$$

Since for $x = 1$ the logarithm on the r.h.s vanishes, the constant must be equal to $\ln p(1)$. Therefore we finally obtain

$$p(x) = Cx^{-\alpha} \tag{2.8}$$

where $C = p(1)$ and $\alpha = -p'(1)/p(1)$. Hence, power laws are the only functions which can be considered scale-free, according to the criterion 2.2.

However, it's worth noticing that in nature this scale invariance is not in general expected to hold for every value of x and b. As a matter of fact, a power law distribution of the form 2.1 diverges for $x \to 0$ (provided that $\alpha > 0$). This suggests that in actual systems, pure power law behavior could be present only down to a lower cutoff x_{min}: scale invariance can be observed only when both x and bx are greater than x_{min}. This deviation from pure power law behavior is shown in Figure 2.3. Generally speaking, an actual distribution $p(x)$ is characterized by deviations from pure power law behavior also for large values of the variable x, which could be related for instance to the finite size of the system. Let's stick to the example of city population in the US. There are only finitely many people living in the US: the population of a US city cannot exceed the population of the whole country. This means

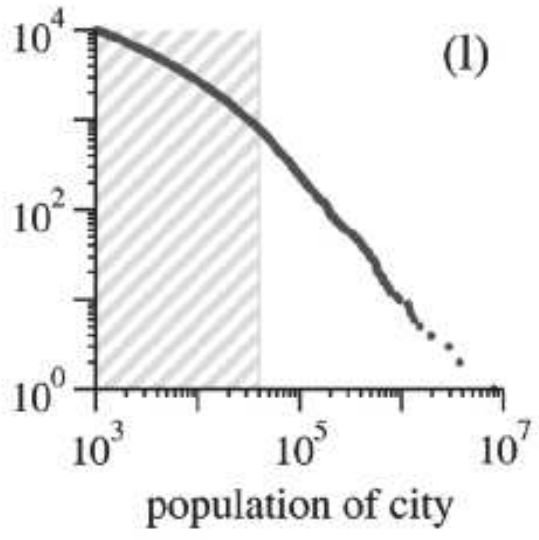

Figure 2.3: Population of US cities in year 2000. The shaded region indicates the range of values for which pure power law behavior is lost: in that region, the graph exhibits a non-zero curvature. In this particular case, the lower cutoff can be estimated to be roughly 40000. Figure from [20].

that also an upper cutoff x_{max} defines the range in which pure power law behavior is expected to be observed in real finite-sized systems. The distribution is such that it rapidly decays to zero as x approaches x_{max}.
The property of scale invariance of a power law distribution $p(x)$ must therefore in general be acknowledged to hold only in a finite range of values, approximately between the two cutoffs x_{min} and x_{max} that were defined before. However, it should be kept in mind that the range of validity is usually found to span several orders of magnitude, as can be seen for example in Figure 2.3. The ratio x_{max}/x_{min} in that case is roughly 250. This is certainly a different situation compared to the one of Figure 2.1: the ratio between the height of the tallest and the shortest man is about 4.8 ([20]).

2.1.2 Origin of power laws

The apparent ubiquity of power law distributions in such diverse contexts suggests that there could be a general underlying principle at the origin of

this behavior. In the past, various mechanisms through which power law distributions could arise have been put forward. Some of these mechanisms are fairly simple, such as the combination of exponentials ([20]), which for example was proposed by Miller ([17]) to give an explanation to the power law distribution of word frequency in English language (and actually in any spoken and also any dead language ever developed by humans). Another example is the Yule process ([20]), developed in order to justify the distribution of the number of species in a particular genus, which was then extended to model also the distribution of paper citations, city populations and others.

A peculiar mechanism, which has received more and more attention during the past few decades, is that of critical phenomena. It is known that some systems possess only one characteristic length-scale or time-scale. One example would be the Ising model of a magnet, in which the only length-scale is the correlation length between two spins. By changing the temperature, it is possible to drive the system towards a *critical point*, characterized by a critical value of the temperature usually denoted by T_c, the crossing of which would result in a *phase transition*. As the system approaches the edge of the phase transition, the correlation length is found to increase up to the size of the system: in the thermodynamic limit, it will therefore diverge. Since that is the only length-scale, at the critical point the system is left with no scale at all. Thus, it is expected that physical quantities will be distributed according to scale-free distributions, i.e. power laws.

This scale invariance is however observed only in the vicinity of the criticality: driving the system in such state would imply a fine tuning of the parameters. Since natural systems exhibit scale invariance without the need of this fine tuning, criticality would not seem a plausible explanation for the emergence of power laws.
Yet, it has been proposed that some natural systems automatically arrange themselves in such a way that they're always in the vicinity of a phase transition, a phenomenon that goes under the name of *self-organized criticality* ([19], [20]).

An illustrative example of this mechanism is the Bak-Tang-Wiesenfeld (BTW) model of avalanches. Suppose we have a one-dimensional lattice comprising N sites. In each site, grains of sand can accumulate to form vertical piles of various heights. We indicate with h_i, $i = 1, \ldots, N$ the height of the sandpile at position i, defined as the number of grains piled up in site i. We define also the variable $z_i = h_i - h_{i+1}$, i.e. the height difference between the sandpile at position i and its right nearest neighbor. If z_i exceeds

a certain threshold value $Z > 0$, the sandpile at position i topples: a sand grain is moved from site i to site $i + 1$.

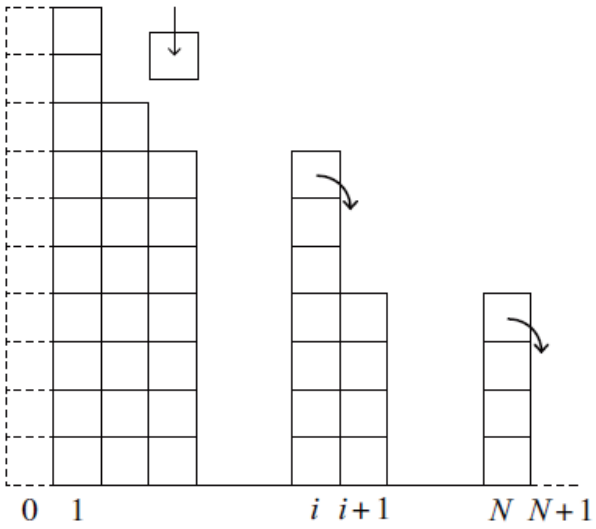

Figure 2.4: The figure shows the three main mechanisms that define the dynamics of the BTW model: the addition of a grain of sand to a random position, the toppling of sandpiles to their right and the ejection of sand grains from the right boundary of the lattice. Figure from [16].

Notice that this toppling process will stop if $z_i < Z$ for every i. When this happens, one additional grain of sand is added to the system and placed on the top of a sandpile in a randomly selected position, in order to make the toppling start again. The boundary conditions are open on the right but not on the left: grains of sand can be ejected from the system by toppling to the right if $h_N > Z$, but they cannot roll from $i = 1$ to the left. The variables we're interested in are the size and duration of *avalanches*, denoted with n and τ respectively. n is defined as the number of sandpiles that topple after the introduction of an additional grain of sand, whereas τ is the number of timesteps required such that the avalanche stops, and the addition of a new grain of sand is needed. In one dimension, the model does not display particularly unexpected features. Starting from an empty system and gradually adding grains of sand at random positions, after a transient time the piles will eventually reach a state in which $z_i = Z$ for every i ([16]). At this point, whenever a new grain is added to the system,

it will topple directly to the right boundary and it will be ejected: the size of the avalanche will be equal to the distance from the randomly selected site over which the grain is added to site N: since the latter site is chosen with a uniform probability among all the N sites, n and τ will be distributed uniformly as well.

On the other hand, in two (or more) dimensions, the model presents very peculiar features: n and τ are found to be distributed according to a power law

$$P(n) \sim n^{-\theta}, \; P(\tau) \sim \tau^{-\eta} \tag{2.9}$$

where $\theta = 0.98$ and $\eta = 0.42$ in two dimensions ([16]).

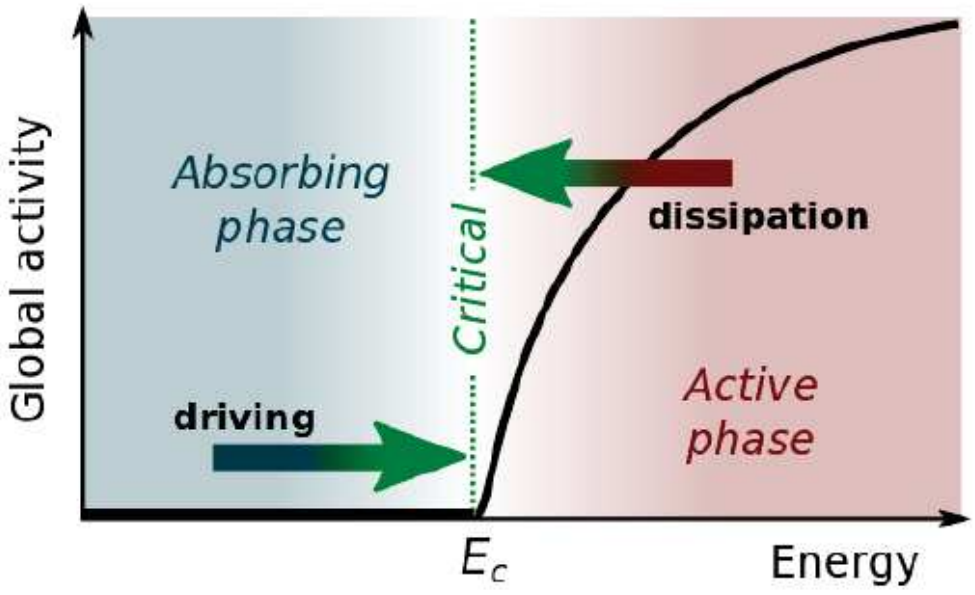

Figure 2.5: A pictorial explanation of the insurgence of self-organized criticality. In the particular case of the BTW model, one may think to have the total number of sand grains on the horizontal axis. Figure from [19].

It is possible to extrapolate some general remarks from the BTW model. We can say that the system can be found in two phases, characterized by their *activity*: in one phase the activity is 0, whereas it is positive in the other (in the case of the BTW model, the activity can be thought of as the

presence of avalanches). The presence of a driving force tends to push the system toward the active phase (addition of grains of sand); on the other hand, dissipation (ejection of grains of sand) works in the opposite direction, since it drives the system toward the inactive phase. This feedback loop ensures that the system adjusts itself in the vicinity of the critical point (see Figure 2.5). An important point is that this adjustment is achieved without the need for a fine tuning of the parameters that govern the dynamics of the system.

The same self-adjusting behavior is observed in many other models regarding biological and ecological systems, in which both driving and dissipative factors are present. The idea that has been put forward is that there could be some functional advantages for biological systems for staying in the vicinity of criticality (e.g. divergence of susceptibility, see [19]): evolution may have shaped organisms in order to exploit these advantages to get the maximum benefits. This could explain the ubiquity of power law distributions in natural systems.

2.2 Modeling forest communities

In this section, we'll present a recently proposed model ([21]) to describe the distributions of several different quantities in the context of forest communities. The model is based on considerations on metabolic efficiency of both individual trees and of the forest as a whole, along with some assumptions regarding the finite-size scaling form of the distributions.

Let's consider a forest covering an area A, which contains a certain number of trees $N \propto A$. The forest is in a steady state, i.e. the number of trees N does not vary over time, as well as the distributions of all the quantities that characterize the forest itself (e.g. the distributions of trunk diameters, tree heights and others, see below). Differences between tree species are neglected. Every tree is characterized by an height h, which is such that $h_0 < h < h_c$: h_0 is a "recruitment" height, so that trees shorter than h_0 are not considered, whereas h_c is the typical height of the tallest trees in the forest. h_0 and h_c are such that $h_0 \ll h_c$. At this point, we introduce four main hypothesis: two of them regard the shape of an individual tree, the others deal with the forest as a whole.

H1: Tree shape There are two main characteristic lengths that determine the shape of a tree, namely the height h and the transverse extension

(or crown radius) r_{cro}. The model postulates that a power law relation exists between these two lengths, i.e.

$$r_{cro} \sim h^H \tag{2.10}$$

with $H > 0$. It is also reasonable to take $H \leq 1$: this is because the ratio r_{cro}/h scales as h^{H-1}, and consequently $H > 1$ would imply that very tall trees are largely more wide than they are tall, an undoubtedly unrealistic picture. $H = 1$ corresponds to an isometric tree shape, in which the ratio r_{cro}/h remains constant for all heights. Instead, for $0 < H < 1$ the ratio r_{cro}/h decreases as h increases: taller trees are proportionally "thinner" than shorter ones.

With this assumption, the total crown volume V scales as

$$V \sim h^{1+2H} \tag{2.11}$$

H2 : Energy optimization of a tree It is assumed that the metabolic rate B of a tree is proportional to the number of leaves, which are the metabolic active sites where photosynthesis takes place. The number of leaves is itself proportional to the crown volume, thus

$$B \sim h^{1+2H} \tag{2.12}$$

H3: Energy optimization of the forest The volume of the forest is postulated to be completely filled by leaves. This ensures that the energy utilized by the forest is maximized. The volume of the forest is proportional to the area A (or equivalently the number of trees N) times the typical height of the tallest trees h_c.

H4: Scaling The tree height distribution is assumed to have a finite-size scaling form of the kind

$$p(h|h_c) = h^{-\alpha} f_h\left(\frac{h}{h_c}\right) \tag{2.13}$$

The function f_h tends to a constant value when $h/h_c \ll 1$, whereas it rapidly goes to zero as the argument approaches 1. In this way, the distribution displays a pure power law behavior when one considers small and intermediate heights, which is then cut off by approaching h_c.

2.2.1 Metabolic optimization

Firstly, we're going to deduce the metabolic rate - mass relation. In order to do that, we will exploit a general theorem for directed transportation networks ([4]). Suppose we have a directed network in which a fluid (e.g. blood or sapwood) is flowing. All the sites are connected through some route to a central site, called *source*. Different examples of such networks are shown in Figure 2.4. The fluid transports nutrients, and each site is supplied with such nutrients at a steady rate. Let's further suppose that the system is in a steady state, i.e. the quantity of nutrients supplied by the source per unit time exactly matches the nutrient demand of all sites of the network. The most efficient networks are the ones in which the fluid volume is as small as possible. The theorem states that, for this efficient class of networks, the fluid volume scales as the number of sites times the average distance between a site and the source. In the case of trees, we can think of the source to be located at the basement of the tree, since sapwood has to be transported from the roots to the leaves, which are the terminal units of the network. The average distance of a leaf from the source scales as the tree height h. Recalling that the number of leaves scales as h^{1+2H} from hypothesis H1, by applying the theorem, the volume of the sapwood (and thus its mass), is proportional to h^{2+2H}. If the mass M of the tree scales isometrically with the mass of the sapwood, then we obtain the relation

$$M \sim h^{2+2H} \tag{2.14}$$

This relation permits to deduce the scaling form of other quantities with tree height h, for instance the trunk diameter and the metabolic rate B. For what concerns the trunk diameter, denoted henceforth with r, empirical data show that M scales as the trunk volume r^2h. Therefore one finds

$$r \sim h^{\frac{1+2H}{2}} \tag{2.15}$$

Also, from assumption H2 it immediately follows that

$$B \sim M^{\frac{1+2H}{2+2H}} \tag{2.16}$$

This last equation is of particular importance, since it allows the use of an optimization principle for B: we will choose H in such a way that B is maximized for a given mass M. The function at the exponent is monotonically increasing for all $H > 0$. Hence, because we have assumed that $0 < H \leq 1$

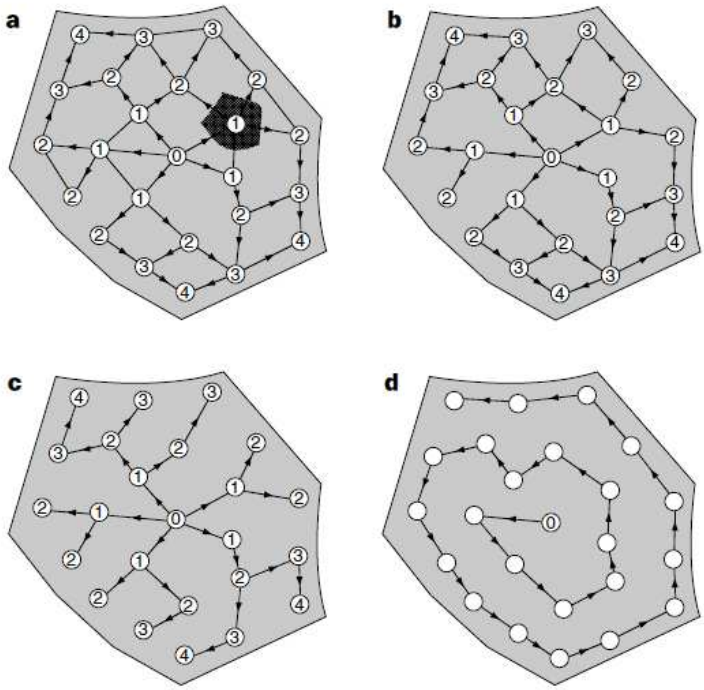

Figure 2.6: Different examples of directed transportation networks. The number on each site is a measure of the distance from the source, which is calculated as the number of sites encountered along the shortest route that connects a given site to the source, also counting the site itself. The source is labeled with the number 0. Figure from [4].

with hypothesis H1, the optimal value for H turns out to be $H = 1$. With this principle of metabolic optimization we find again Kleiber's law

$$B \sim M^{3/4} \tag{2.17}$$

Substituting $H = 1$ also in the other scaling relations found before, we obtain for example $r \sim h^{3/2}$ and $B \sim r^2$. These results are in good accord with empirical data, and this gives credit to the assumption that the mass of the sapwood scales isometrically with tree mass M.

2.2.2 Relations between exponents

A useful observation deals with the volume of the forest, which is equivalent to the total number of leaves of all trees since we have assumed that the volume is completely filled (H3). There are two measures of this volume: one is simply $A \cdot h_c$, whereas the other is given by the number of trees with heigths between h and $h + dh$ times the number of leaves of such trees, integrated over all heigths

$$Ah_c \propto A \int_{h_0}^{+\infty} dh p_h(h|h_c) h^{1+2H} \tag{2.18}$$

We can make the change of variables $x = h/h_c$ and obtain

$$\begin{aligned} Ah_c &\propto Ah_c^{2+2H-\alpha} \int_{h_0/h_c}^{+\infty} dx x^{-\alpha} f_h(x) \\ &\simeq Ah_c^{2+2H-\alpha} \int_0^{+\infty} dx x^{-\alpha} f_h(x) \end{aligned} \tag{2.19}$$

where the last step is justified by the fact that we have assumed $h_0 \ll h_c$. The integral does not depend on h_c, so it can be included in the proportionality constant. Therefore we obtain a relation between α and H, i.e.

$$\alpha = 1 + 2H \tag{2.20}$$

Notice that we're proceeding without assuming a particular value for the exponent H. Using assumptions H1, H3 and H4, we have been able to find a relation between two quantities that belong to different domains: H is an exponent that characterizes the shape of an individual tree, whereas α is related to the whole forest structure.

At this point one could ask what the distribution would look like for a variable related to the tree height h by a power law with an exponent ω. In general, let x and y be two positive random variables related by a power law

$$y \sim x^{\omega} \tag{2.21}$$

and let x be distributed according to

$$p(x|x_c) = x^{-\alpha} f_x\left(\frac{x}{x_c}\right) \tag{2.22}$$

where f_x has the properties discussed for hypothesis H4. Suppose now that the conditional probability of y given x, denoted with $P_y(y|x)$, satisfies

$$P_y(y|x) = \frac{1}{y} F_y\left(\frac{y}{x^\omega}\right) \tag{2.23}$$

One can compute the n-th moment of y

$$\langle y^n \rangle = \int dy y^n P_y(y|x) = \int dy y^{n-1} F\left(\frac{y}{x^\omega}\right) \tag{2.24}$$

With the change of variables $z = y/x^\omega$ one gets

$$\langle y^n \rangle = c_n x^{\omega n} \tag{2.25}$$

where

$$c_n = \int dz z^{n-1} F(z) \tag{2.26}$$

Equation 2.25 is the generalization of the deterministic relation $y = x^\omega$ to a more general case in which the n-th moment of y scales as $x^{\omega n}$. Henceforth, when we say that two variables x and y are related by a power law, we will actually mean that the probability of y conditioned to x has the form of equation 2.25. At this point, one can proceed to the derivation of the distribution $p_y(y|y_c)$.

$$p_y(y|x_c) = \int dx P_y(y|x) p_x(x|x_c) = \int dx \frac{1}{y} F_y\left(\frac{y}{x^\omega}\right) x^{-\alpha} f_x\left(\frac{x}{x_c}\right) \tag{2.27}$$

If we perform the change of variables $z = x/y^{1/\omega}$, the integral becomes

$$p_y(y|x_c) = y^{-\frac{\alpha+\omega-1}{\omega}} \int dz z^{-\alpha} F_y(z^\omega) f_x\left(\frac{z y^{1/\omega}}{x_c}\right) \tag{2.28}$$

If we define $y_c = x_c^\omega$, the integral in the previous equation depends on y and y_c only through the ratio y/y_c. It is possible therefore to define

$$f_y\left(\frac{y}{y_c}\right) = \int dz z^{-\alpha} F_y(z^\omega) f_x\left(z\left(\frac{y}{y_c}\right)^{1/\omega}\right) \tag{2.29}$$

thus obtaining the result

$$p_y(y|y_c) = y^{-\frac{\alpha+\omega-1}{\omega}} f_y\left(\frac{y}{y_c}\right) \tag{2.30}$$

Equation 2.30 correspond to the finite size scaling for the distribution of y, and we see that the definition of y_c allows to identify it as the upper cutoff. If we replace the variable x with tree height h, then $\alpha = 1 + 2H$. At this point, one can deduce the distributions for all the quantities related to tree height h by a power law. Let's consider some examples.

We know that the trunk diameter r is related to the tree height by the power law 2.15. Thus in this case $\omega = (1 + 2H)/2$. Using equation 2.30, the distribution of trunk diameters is given by

$$p_r(r|r_c) = r^{-\frac{1+6H}{1+2H}} f_r\left(\frac{r}{r_c}\right) \tag{2.31}$$

where $r_c = h_c^{\frac{1+2H}{2}}$. The particular choice of the optimal value $H = 1$ yields an exponent of -7/3. Likewise, from equation 2.14, the distribution of tree masses is predicted to be

$$p_M(M|M_c) = M^{-\frac{1+2H}{1+H}} f_M\left(\frac{M}{M_c}\right) \tag{2.32}$$

with $M_c = h_c^{2+2H}$, which exponent becomes -3/2 when $H = 1$. Generally speaking, given a variable related to tree height h with a power law which exponent is known, equation 2.30 permits to deduce its distribution, which has the same finite-size scaling form of the height distribution in hypothesis H4.

2.2.3 Range of influence

A variable of particular interest is the *range of influence*, denoted with r_i. This is defined as the distance from a given tree to the nearest tree having a larger diameter. Because of competition for space (and, consequently, light), it is expected that

$$r_i \sim r_{cro} \sim h^H \tag{2.33}$$

Using the same procedure explained in the previous section, since in this case $\omega = H$ the distribution of r_i is

$$p_{r_i}(r_i|r_{i,c}) = r_i^{-3} f_{r_i}\left(\frac{r_i}{r_{i,c}}\right) \tag{2.34}$$

which exponent does not depend on the particular value of H. We now introduce the cumulative PDF $P^{>}_{r_i}(r_i|r_{i,c})$, which is the fraction of trees whose range of influence is greater than r_i. This is given by

$$P^{>}_{r_i}(r_i|r_{i,c}) = \int_{r_i}^{+\infty} dr_i'(r_i')^{-3} f_{r_i}\left(\frac{r_i'}{r_{i,c}}\right) \tag{2.35}$$

We can perform the change of variables $x = r_i'/r_{i,c}$ and obtain

$$P^{>}_{r_i}(r_i|r_{i,c}) = r_{i,c}^4 \int_{r_i/r_{i,c}}^{+\infty} dx x^{-3} f_{r_i}(x) \tag{2.36}$$

Now the function $f_{r_i}(x)$ tends to a constant value when $x \ll 1$, whereas it rapidly decays to 0 as x approaches 1. Thus, if $r_i \ll r_{i,c}$, the major contribution to the integral in the previous equation will come from the region in which f_{r_i} is constant. Therefore the cumulative PDF is expected to scale as

$$P^{>}_{r_i}(r_i|r_{i,c}) \sim r_i^{-2} \tag{2.37}$$

when $r_i \ll r_{i,c}$. As r_i approaches $r_{i,c}$, this pure power law behavior should eventually disappear as the cumulative PDF should rapidly go to zero.

However, as can be observed in Figure 2.7, the pure power law behavior holds up to distances of the order of hundreds of meters, certainly much larger than $r_{i,c}$, which ought to be approximately the same as h_c. Why is this the case? When considering distances greater than $r_{i,c}$, one may assume a random distribution of trees in the forest. In order to have some insights about why the power law 2.37 extends much beyond the expected range, let us consider an area A on the $x - y$ plane, in which N points (trees) are uniformly distributed. Each point is endowed with a random number (diameter) picked from a certain distribution. What is the cumulative PDF of the range of influence in this random scenario? Figure 2.8 shows that indeed $P^{>}_{r_i}(r_i) \sim r_i^{-2}$ for intermediate and large values of r_i: this is the same exponent found following the scaling hypothesis. For small values of the range of influence r_i, the dimension of tree crowns matter, and the scaling framework is the most adequate. For large values of r_i instead, one can apply random distribution considerations. However, the values of the scaling

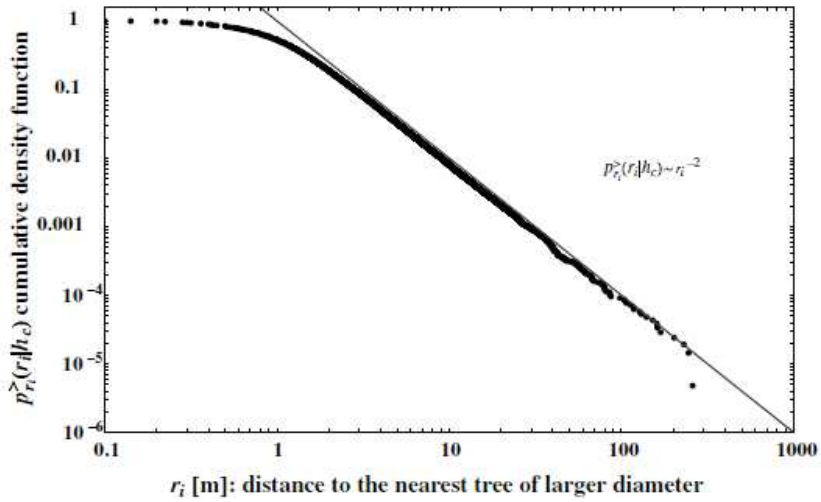

Figure 2.7: Cumulative PDF for the range of influence r_i (measured in meters) for the Barro Colorado Island forest (1995 census). The pure power law behavior is observed far further than $r_{i,c}$, up to roughly 200 m. Figure from [21].

exponents obtained in the two cases match: this ensures that there is very little need for an upper cutoff for the distribution $p_{r_i}(r_i|r_{i,c})$. For an analytical derivation of the exponent for a random forest, see Appendix A.

The fact that the scaling exponent for small values of r_i matches with the one obtained from random considerations suggests an interesting remark. In a sense, we could argue that trees have somehow *exploited* randomness for structuring their communities. This is not a trivial point, because there is no *a priori* reason for which a random configuration ought to be advantageous from an evolutionary point of view. One possibility could be that, given the inevitability of the laws of chance in Nature, fighting against them required a larger effort than trying to follow them.

2.2.4 Collapse plot

Given two positive random variables x and y related by equation 2.23, it is expected that by plotting $yP_y(y|x)$ against y/x^{ω}, a single curve would be obtained for all the values of x, i.e. all the curves for different values of x

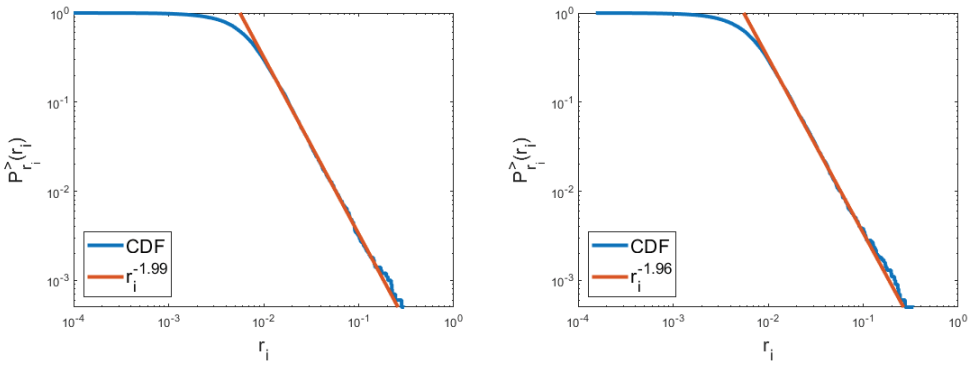

Figure 2.8: (Left panel) Cumulative density function for the range of influence in a "forest" comprising 10^4 trees. Trees are uniformly distributed in a 1×1 square. Tree diameters are assigned randomly from a uniform distribution. Each diameter can be any real number between 0 and 10^3. The slope of the red straight line is found to be -1.985, very close to the value of -2 obtained from the scaling hypothesis. (Right panel) In this case, diameters are assigned starting from a Gaussian distribution with zero mean and unit variance. The simulation in this case yields an exponent of -1.9632. It is evident that there are no significant modifications when one considers different diameter distributions.

would *collapse* onto a single one. This collapse could equivalently be observed by looking at the cumulative distribution $P_y^>(y|x)$, defined as

$$P_y^>(y|x) = \int_y^{+\infty} dy' P_y(y'|x) = \int_y^{+\infty} dy' \frac{1}{y'} F_y\left(\frac{y'}{x^\omega}\right) \tag{2.38}$$

This is because the simple change of variables $z = y'/x^\omega$ yields

$$P_y^>(y|x) = \int_{y/x^\omega}^{+\infty} dz \frac{1}{z} F_y(z) \tag{2.39}$$

which depends on x and y uniquely through the ratio y/x^ω. However, it has to be noted that the collapsing of curves for different values of x onto a single one could be observed only for the values of x for which equation 2.23 holds. Therefore, a collapse plot would be of great utility for testing the scaling hypothesis, checking the values of the exponents and also identifying the ranges of validity of pure power law behavior for the variable x.

As an example, let's consider the range of influence r_i and the tree diameter r. In the particular case of $H = 1$, $r_i \sim h$ whereas $r \sim h^{3/2}$: hence, it is expected that $r_i \sim r^{2/3}$. Figure 2.9 shows that predictions are actually verified by empirical data.

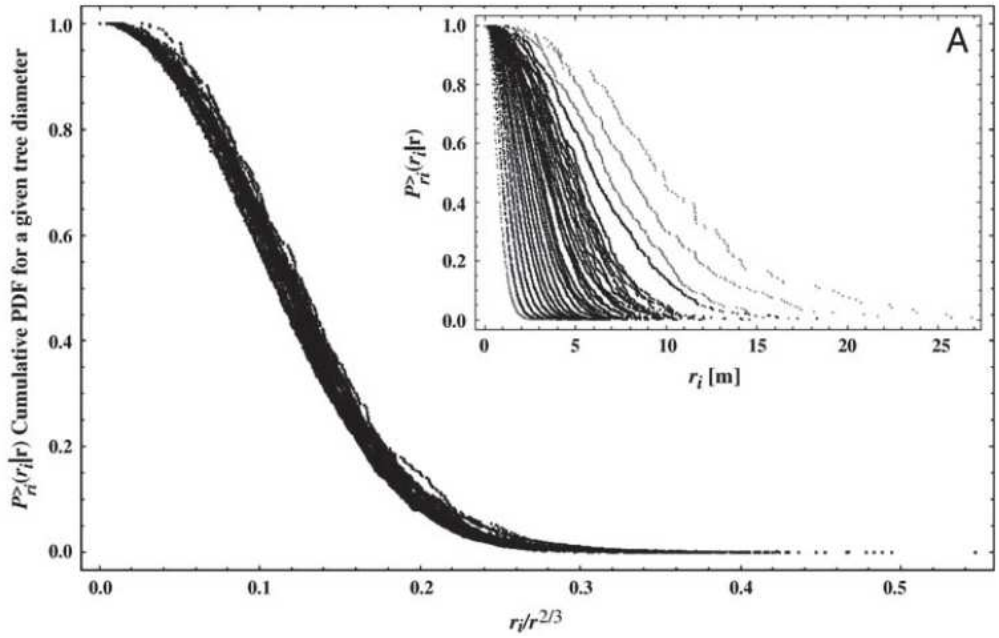

Figure 2.9: Collapse plot for the range of influence r_i of trees of different diameter r in the Barro Colorado Island forest. Figure from [21].

To construct the curve in Figure 2.9, trees were binned in 1 cm size classes, and the cumulative distribution $P^{>}_{r_i}(r_i|r)$ was computed for each one of these classes (curves are shown in the inset). r ranges between 1.4 and 49.4 cm. When the same distribution is plotted against the quantity $r_i/r^{2/3}$, data actually collapse onto a single curve, depicted in the main figure. However, this happens only for values of r from 2.4 up to 31.8 cm. This is the range in which the pure power law behavior for the diameter distribution $p_r(r|r_c)$ is expected to hold. All the predictions (at least the ones regarding the tree diameter r) find confirmation in the curve shown in Figure 2.10: the scaling hypothesis holds in the predicted range, and the value of the exponent actually confirms the optimal value of 1 calculated for H. Anyway, the collapsing procedure described so far can be used for any variable for which

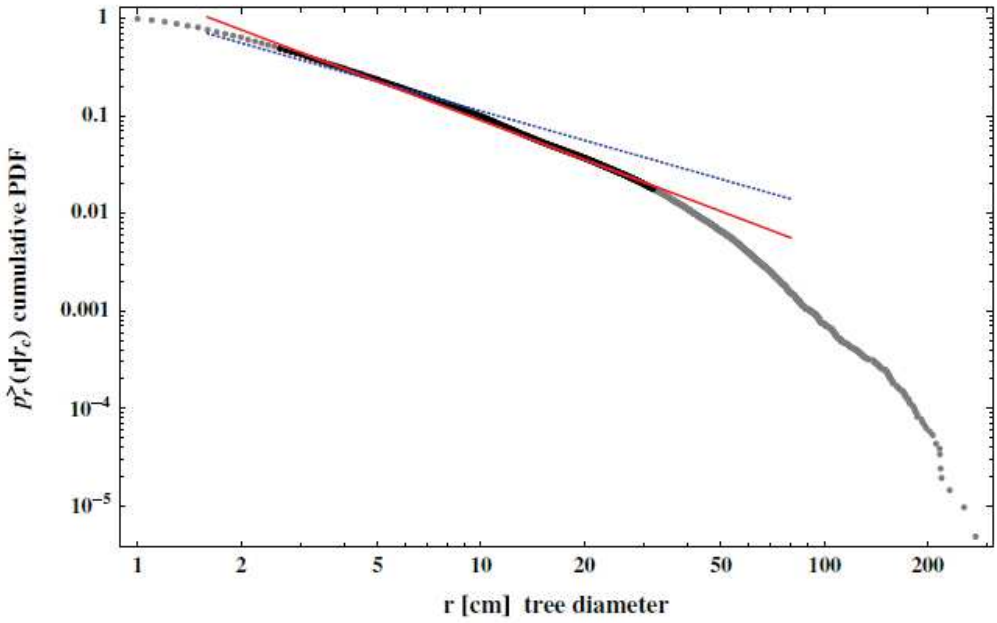

Figure 2.10: Cumulative distribution for the tree diameter r in the Barro Colorado Island forest. Blackened dots belong to the range in which pure power law behavior is expected to hold according to the results of the collapsing procedure shown in Figure 2.9. The red solid line indicates an exponent of -4/3, the one expected from a pdf with exponent -7/3. Figure from [21].

a power law relation with r_i can be established.

2.2.5 Self-similar model

The results obtained so far within the finite-size scaling framework are reproduced by a simple analytically solvable model of a self-similar forest. We're going to present a 2-dimensional version of this model, and then briefly discuss the generalization to 3 dimensions, which is quite straightforward. Let's consider a forest of spatial extent L and such that the height of the tallest trees is h_c, with $L \gg h_c$. This can be represented by a rectangle with base L and height h_c as shown in Figure 2.11.

We will gradually fill the rectangle with smaller and smaller trees such that the whole area of the rectangle will eventually be filled. At zeroth step

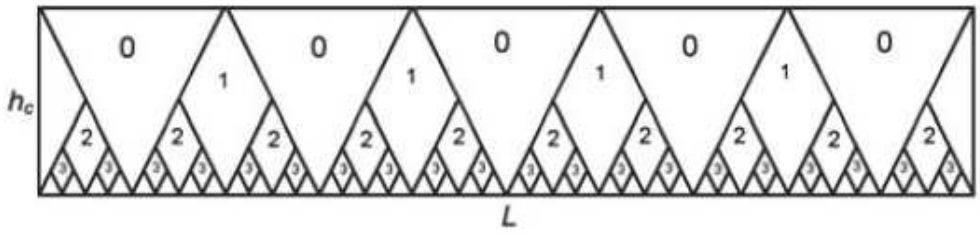

Figure 2.11: Self-similar model of a 2-dimensional forest of spatial extent L and critical height for the tallest trees h_c. Figure from [21].

$(t = 0)$, we introduce the tallest trees of the forest. They can be thought as upside down triangles with base h_c and height h_c. There are $N(0) = L/h_c$ such trees. At step $t = 1$, trees are rhombuses with the longer and shorter diagonals equal to h_c and $h_c/2$, respectively. At step $t = 2$, new smaller rhombuses are added. The height of trees at step $t \geq 1$, which we indicate with $h(t)$, is given by

$$h(t) = \frac{h_c}{2^{t-1}} \tag{2.40}$$

whereas the crown radius $r_{cro}(t)$ is

$$r_{cro}(t) = \frac{h_c}{2^t} \tag{2.41}$$

The number of trees at generation t is given by.

$$N(t) = \frac{L}{h_c} 2^{t-1} \tag{2.42}$$

Notice that the ratio

$$\frac{h(t)}{r_{cro}(t)} = 2 \tag{2.43}$$

for every $t \geq 1$. This implies that the height and the transverse extension of trees scales isometrically, which is equivalent to fixing $H = 1$. Moreover, with this particular construction the volume of the forest (in this case, the area of the rectangle) is completely filled by leaves, satisfying hypothesis H3.

It is now possible to derive the distribution of tree heights, tree metabolic rates and so on. Let us compute the total number of trees in the forest at step t, denoted by $N^{>}(t)$. The latter is given by

$$\frac{L}{h_c}\sum_{s=1}^{t} 2^{s-1} + \frac{L}{h_c} = \frac{L}{2h_c}\left[\sum_{s=0}^{t} 2^s - 1\right] + \frac{L}{h_c} = \frac{L}{h_c}2^t \tag{2.44}$$

From here, it is possible for example to derive the total number of trees taller than h, i.e. $N^{>}(h)$

$$N^{>}(h) = \frac{L}{h_c}2^t = \frac{L}{h_c}\frac{2h_c}{h}\theta(h_c - h) = \frac{2L}{h}\theta\left(1 - \frac{h}{h_c}\right) \tag{2.45}$$

where θ is the Heaviside step function. At this point, in order to compute the distribution $p_h(h|h_c)$, it is sufficient to recognize that

$$p(h|h_c) \propto -\frac{d}{dh}N^{>}(h) \propto \frac{1}{h^2}\theta\left(1 - \frac{h}{h_c}\right) \tag{2.46}$$

thus obtaining a distribution with the finite-size scaling behavior described in hypothesis H4. The same procedure can be carried out for the distributions of all the quantities that have been mentioned in the previous sections. Clearly, the values of the exponents do not coincide since we're considering a 2-dimensional forest. Is it possible to generalize these results to a 3-dimensional forest: in this case, the forest is a square-based prism with an $L \times L$ base and height h_c. Trees are modeled as squared bipyramids. Similar results are found also in the 3-dimensional case ([21]) and the values of the exponents coincide with the ones obtained from the analysis of the previous sections.

2.3 Ecological implications

The model presented in Section 2.2 is definitely a useful tool for making predictions about the structure of natural steady-state forests, as the matching with empirical data confirms. This has both theoretical and practical implications for Ecology. From a theoretical perspective, this model highlights the pivotal role of the metabolic requirements of individuals in the structure of a community. The relation between the exponent H and α bridges the biological features of a single tree to the ecological properties of the whole

population. A linkage of this kind was already encountered in Chapter 1 talking about Damuth's law for population density. This remarks the importance of achieving a complete and detailed understanding of the 3/4 power scaling of metabolic rate in living organisms, given the significance it has for ecosystems. From a more practical point of view, a detailed comprehension of the structure of natural forests has important implications for the entire planet Earth. As a matter of fact, forests are a central component of the global carbon cycle (trees are CO_2 consumers): understanding the extent to which tree communities alter this cycle allows to make predictions for instance about the "safe" level of carbon dioxide emissions from anthropogenic activities ([10]). Also, the fact that the results of this chapter were obtained for natural forests permits to assess the degree of disturbance in a certain ecosystem: if a natural forestal ecosystem has been in some way disturbed by human activity, by measuring for instance the diameter distribution it is possible to compare it with the distribution expected for a natural forest. The closest the two distributions, the closest the forest is to a full recover after the introduction of the disturbance ([3]).

Chapter 3

Allometry of *in vitro* systems

In this chapter, some recent ideas concerning the allometric scaling of *in vitro* cell constructs will be presented. In particular, the model proposed in [1] will be analyzed and discussed. Some of the assumptions will be modified to check the effect this has on the system.

3.1 Body-on-a-chip

In the past decade, cell biology has experienced a technological revolution. This has been primarily due to the production of new experimental devices for *in vitro* cell cultures that permit to mimic more and more precisely the conditions of cells in the *in vivo* environment ([18],[22]). The novel and intriguing idea of a body-on-a-chip has stemmed from these technological advancements: under proper conditions, it would seem possible to prepare an *in vitro* system which could be representative of a real organism. This would allow to get some insights about the functioning of groups of cells and also about the interactions between different cell types, with the aim of extrapolating the experimental results to human physiology. This is a promising approach for instance for *in vitro* drug testing: it could be possible to eliminate therapies that have toxic side-effects, together with expensive clinical trials ([18]).

Allometric scaling has been recognized as a suitable theoretical framework for designing such systems ([1],[18],[22]). Let's for example consider Kleiber's law 1.2. If the whole-body basal metabolic rate B scales as $M^{3/4}$, then

$$\frac{B}{M} \sim M^{-1/4} \tag{3.1}$$

This means that the basal metabolic rate *per cell* decreases as M increases. This is a feature that has to be taken into account when downscaling an organism. As can be observed in Figure 3.1, a first issue in this

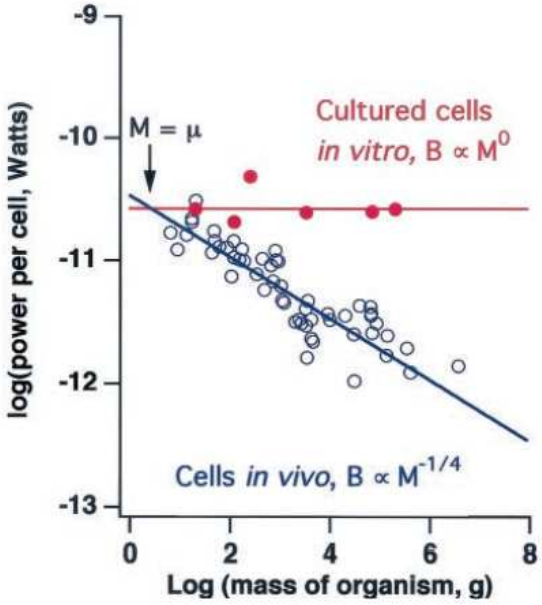

Figure 3.1: Comparison of metabolic rate per cell in *in vivo* and *in vitro*. For *in vivo* cells Kleiber's law holds. On the other hand, data from cultured cells do not display any mass dependence. Figure from [25].

downscaling procedure is the fact that the metabolic rate per cell does not seem to obey the expected allometric scaling law. This may be due to the 3/4 scaling law in actual living organisms being related to the structure of the resources distribution network, which is not mirrored in *in vitro* constructs ([18]). A greater predictive power would be achieved if the system followed the quarter-power scaling predicted by Kleiber's law ([1],[18]). To this date, there have not been successful attempts yet, and the translational potential to human body of these systems is still limited. In order to achieve the quarter-scaling explained before, one strategy consists in the modulation of the oxygen supply to the construct in order to control its metabolic

consumption ([1],[18]).

3.1.1 The model

We now turn our attention to the model presented in [1], which aims to determine the allometric scaling relation of an *in vitro* system by taking into account also parameters such as oxygen supply. Let's consider a spherical cell construct of radius R within an oxygen bath. Cell density ρ is assumed to be uniform. The oxygen concentration outside the sphere is by some means kept at a constant value c_0. Let's assume that oxygen molecules diffuse once they've entered the sphere. Furthermore, let us hypothesize that oxygen consumption is regulated by a Michaelis-Menten kinetics (see Appendix B). From these assumptions, the variation of the concentration $c(\vec{r}, t)$ with respect to time t is given by the sum of two contributions

$$\frac{\partial c(\vec{r}, t)}{\partial t} = D\nabla^2 c(\vec{r}, t) - v_{max}\frac{c(\vec{r}, t)}{k_m + c(\vec{r}, t)} \tag{3.2}$$

where $\vec{r}$ is measured from the center of the sphere. D indicates the diffusion coefficient of oxygen in water, whereas v_{max} and k_m are two parameters of Michaelis-Menten kinetics: v_{max} is the maximum velocity of the reaction, k_m is the so-called *Michaelis-Menten constant*, and it is characteristic of the enzyme and the substrate that participate in the reaction. We will consider the stationary state, so that the equation becomes

$$D\nabla^2 c(\vec{r}) = v_{max}\frac{c(\vec{r})}{k_m + c(\vec{r})} \tag{3.3}$$

We can now turn to spherical coordinates: by exploiting the spherical symmetry of the system one obtains

$$\frac{D}{r^2}\frac{\partial}{\partial r}\left[r^2\frac{\partial c(r)}{\partial r}\right] = v_{max}\frac{c(r)}{k_m + c(r)} \tag{3.4}$$

where $r = |\vec{r}|$. Since the oxygen concentration must be c_0 outside the sphere, one boundary condition is $c(R) = c_0$. It is possible to rewrite the previous equation in a more manageable form by rescaling variables in the following way

$$\lambda = \frac{r}{R},\ \hat{c} = \frac{c}{c_0},\ \kappa = \frac{k_m}{c_0} \tag{3.5}$$

The dimensionless equation obtained after performing this change of variables is

$$\frac{1}{\lambda^2}\frac{\partial}{\partial\lambda}\left[\lambda^2\frac{\partial\hat{c}(\lambda)}{\partial\lambda}\right] = \beta^2\kappa\frac{\hat{c}(\lambda)}{\kappa+\hat{c}(\lambda)} \tag{3.6}$$

where $\beta = \sqrt{\frac{v_{max}}{Dk_m}}R$ and the condition $c(R) = c_0$ translates into $\hat{c}(1) = 1$. At this point, one can expand the l.h.s. and finally get

$$\frac{\partial^2\hat{c}(\lambda)}{\partial\lambda^2} + \frac{2}{\lambda}\frac{\partial\hat{c}(\lambda)}{\partial\lambda} = \beta^2\kappa\frac{\hat{c}(\lambda)}{\kappa+\hat{c}(\lambda)} \tag{3.7}$$

This equation presents the advantage of depending only upon two parameters, i.e. β and κ. Once the concentration is known, it is possible to determine the metabolic rate B (measured in mol/s) as the net inward flux of oxygen in the sphere, i.e.

$$B = 4\pi R^2 D\frac{\partial c(r)}{\partial r}\bigg|_{r=R} = 4\pi D c_0 R\frac{\partial\hat{c}(\lambda)}{\partial\lambda}\bigg|_{\lambda=1} \tag{3.8}$$

Another quantity which can be studied is the total number of moles in the sphere, denoted with n, obtained by integrating the concentration

$$n = 4\pi\int_0^R drr^2c(r) = 4\pi c_0R^3\int_0^1 d\lambda\lambda^2\hat{c}(\lambda) \tag{3.9}$$

Unfortunately, equation 3.7 cannot be solved analytically. However, it is possible to get some insights by considering two particular limits, namely $\hat{c} \ll \kappa$ and $\hat{c} \gg \kappa$ for every $\lambda \in [0, 1]$.

Case 1: $\hat{c} \ll \kappa$
In this particular limit, $\hat{c}$ becomes negligible with respect to κ and can be therefore erased from the denominator of the r.h.s. of equation 3.7. Thus it is possible to write

$$\frac{\partial^2\hat{c}(\lambda)}{\partial\lambda^2} + \frac{2}{\lambda}\frac{\partial\hat{c}(\lambda)}{\partial\lambda} = \beta^2\hat{c}(\lambda) \tag{3.10}$$

This is an equation that can be solved analytically for example by introducing the quantity $y(\lambda) = \lambda\hat{c}(\lambda)$. With this substitution, the equation becomes

$$\frac{\partial^2 y(\lambda)}{\partial \lambda^2} = \beta^2 y(\lambda) \tag{3.11}$$

with $y(1) = 1$. A general solution is given by

$$y(\lambda) = A_1 e^{\beta\lambda} + A_2 e^{-\beta\lambda} \tag{3.12}$$

Given the definition of the function $y(\lambda)$, it immediately follows that

$$\hat{c}(\lambda) = \frac{A_1 e^{\beta\lambda} + A_2 e^{-\beta\lambda}}{\lambda} \tag{3.13}$$

At this point, if one wants to avoid the divergence in $\lambda = 0$, the only way is to set $A_1 = -A_2$, which is the choice that has been made in [1]. By further imposing the condition $\hat{c}(1) = 1$, one gets

$$\hat{c}(\lambda) = \frac{1}{\lambda} \frac{\sinh(\beta\lambda)}{\sinh(\beta)} \tag{3.14}$$

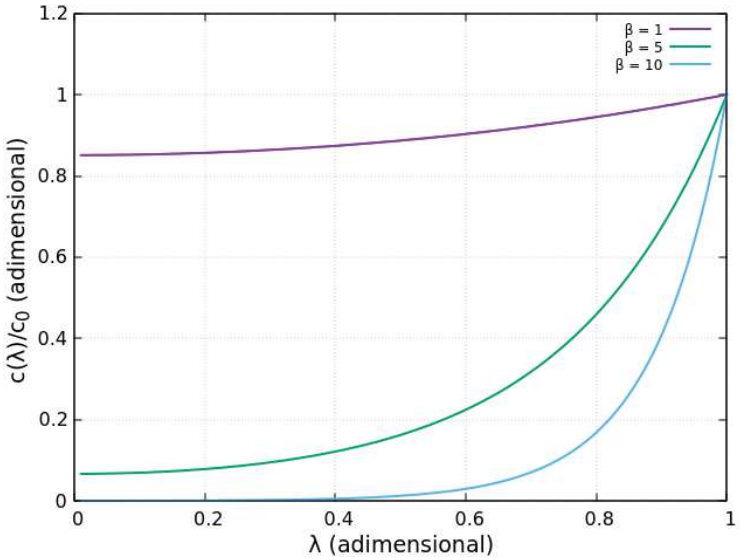

Figure 3.2: $\hat{c}(\lambda)$ in the case $\hat{c} \ll \kappa$ for three different values of the parameter β, namely $\beta = 1, 5, 10$.

The profile of the solution is shown in Figure 3.2. It has to be mentioned that it is necessary to assume also $\kappa \gg 1$ in order for the approximation to be

valid in the complete range $[0, 1]$. According to equation 3.8, the metabolic rate within this approximation is

$$B = 4\pi D c_0 R \left[\frac{\beta}{\tanh \beta} - 1 \right] \tag{3.15}$$

In order to determine the allometric scaling relation, one must express B in terms of the volume V of the sphere (which is itself proportional to the sphere mass M, since we have assumed a uniform cell density). Let's focus on the quantity β

$$\beta = \sqrt{\frac{v_{max}}{D k_m}} R = \sqrt{\frac{v_{max}}{D k_m}} \left(\frac{3}{4\pi} \right)^{1/3} V^{1/3} = (\beta' V)^{1/3} \tag{3.16}$$

where we have introduced

$$\beta' = \frac{3}{4\pi} \left(\frac{v_{max}}{D k_m} \right)^{3/2} \tag{3.17}$$

which, if all the parameters are scale invariant, does not depend on the sphere's size.

At this point one can write

$$\hat{B} = B \sqrt{\frac{v_{max}}{(4\pi)^2 D^3 c_0^2 k_m}} = (\beta' V)^{1/3} \left[\frac{(\beta' V)^{1/3}}{\tanh(\beta' V)^{1/3}} - 1 \right] \tag{3.18}$$

A plot of $\hat{B}$ as a function of $\beta' V$ is shown in Figure 3.3. As highligthed in the latter figure, the metabolic rate scales isometrically with the volume for small values of V, whereas for large V the scaling exponent becomes 2/3. It is also possible to calculate the total number of moles n by using equation 3.9

$$n = 4\pi c_0 R^3 \int_0^1 d\lambda \lambda^2 \hat{c}(\lambda) = \frac{4\pi c_0 R^3}{\beta^2} \left[\frac{\beta}{\tanh \beta} - 1 \right] \tag{3.19}$$

From the definition of β, it is apparent that

$$n = \frac{k_m}{v_{max}} B \tag{3.20}$$

Since n scales isometrically with B, it also has the same scaling behavior with respect to the volume V.

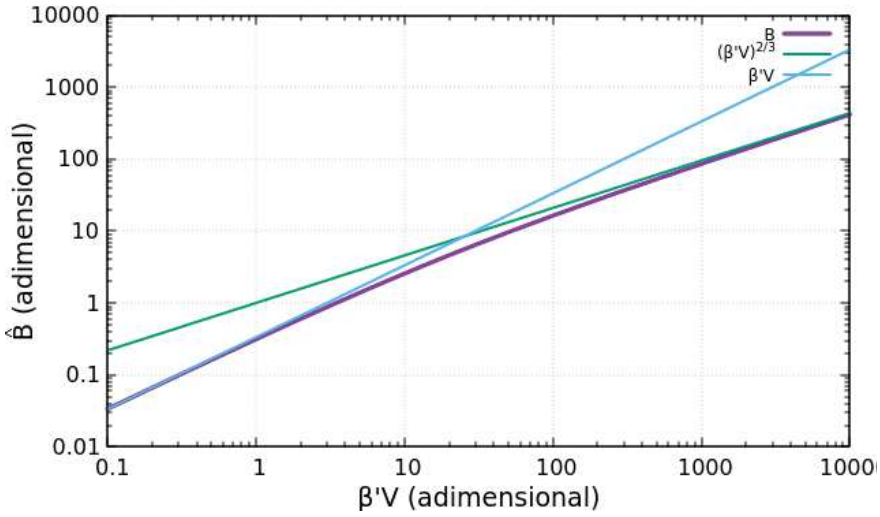

Figure 3.3: $\hat{B}$ as a function of $\beta' V$ (purple line) on a log-log scale. The blue straight line has slope 1, whereas the green one has slope 2/3.

Case 2: $\hat{c} \gg \kappa$

If instead $\hat{c} \gg \kappa$ for every $\lambda \in [0, 1]$, equation 3.7 can be approximated by

$$\frac{1}{\lambda^2}\frac{\partial}{\partial \lambda}\left[\lambda^2 \frac{\partial \hat{c}(\lambda)}{\partial \lambda}\right] = \beta^2 \kappa \tag{3.21}$$

One can multiply both sides by λ^2 and then by integrating twice we obtain

$$\hat{c}(\lambda) = \frac{\beta^2 \kappa}{6}\lambda^2 + C_1 + \frac{C_2}{\lambda} \tag{3.22}$$

Also in this case, in order to avoid divergence in the concentration one has to take $C_2 = 0$. The constant C_1 is instead fixed by the condition $\hat{c}(1) = 1$, which leads to the particular solution

$$\hat{c}(\lambda) = 1 - \frac{\beta^2 \kappa}{6}(1 - \lambda^2) \tag{3.23}$$

This is a parabola with its vertex placed at $\lambda = 0$: the minimum therefore is given by $\hat{c}(0) = 1 - \beta^2\kappa/6$. Since $\hat{c}(\lambda)$ must be positive for every value of $\lambda \in [0, 1]$, we need to require that $\beta^2 \kappa < 6$. Therefore, the approximation

$\hat{c} \gg \kappa$ is only expected to hold for small volumes ($\beta \propto R$). Also, since $\hat{c}(1) = 1$, we need to require $\kappa \ll 1$.

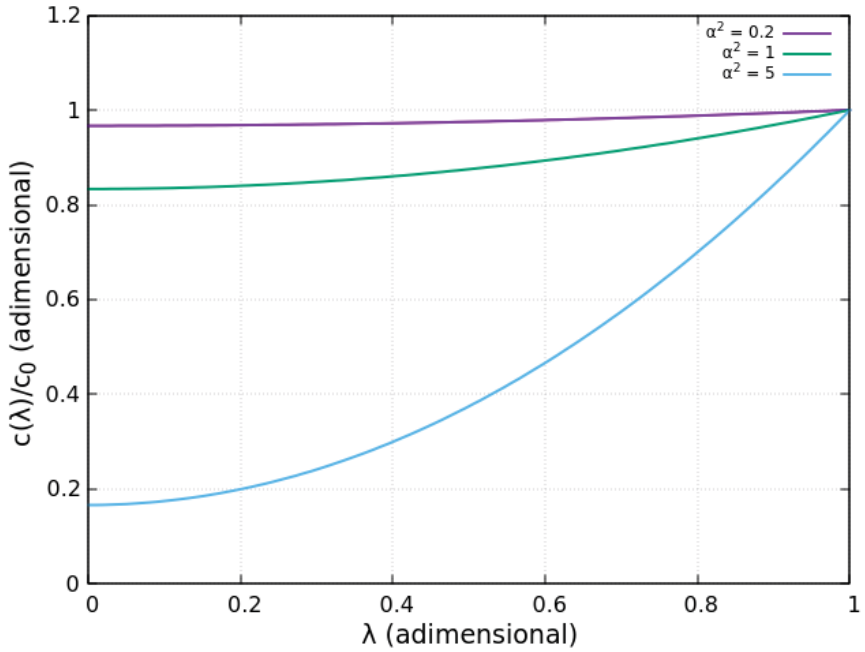

Figure 3.4: $\hat{c}(\lambda)$ as a function of λ in the approximation $\hat{c} \gg \kappa$ for three different values of $\beta^2\kappa$, all satisfying the condition $\beta^2\kappa < 6$. In the figure, $\alpha^2 = \beta^2\kappa$.

It is now possible to compute the metabolic rate B from equation 3.8

$$B = v_{max}V \tag{3.24}$$

In this case, B scales isometrically with V for all the values of V such that $\beta^2\kappa < 6$. The integral of the concentration yields

$$n = \frac{4}{3}\pi c_0 R^3 \left[1 - \frac{\beta^2\kappa}{15}\right] \tag{3.25}$$

The last equation can be rewritten in terms of the volume V by introducing the parameter

$$\alpha' = \frac{3}{4\pi}\left(\frac{v_{max}}{Dc_0}\right)^{3/2} \tag{3.26}$$

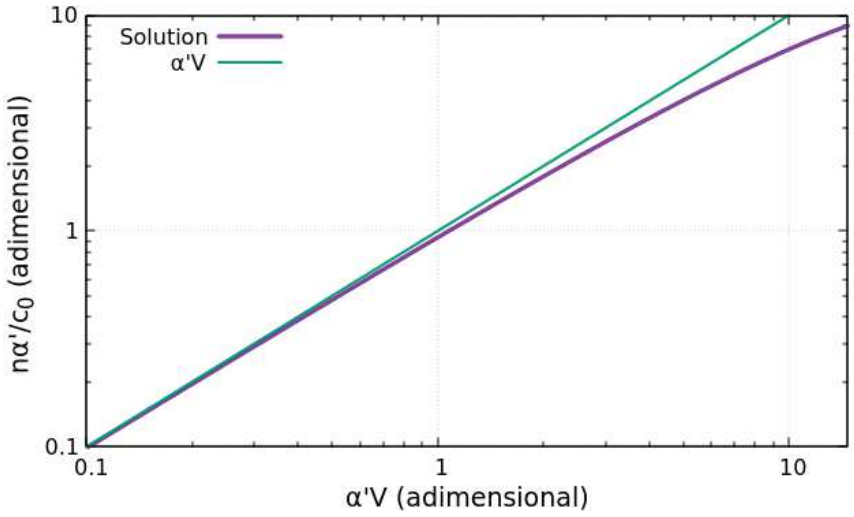

Figure 3.5: $\hat{n}$ as a function of the dimensionless parameter $\alpha' V$ in the range specified by the condition $\alpha' V < 6^{3/2}$. The green straight line has slope 1.

which has the dimensions of the inverse of a volume. It is then possible to write

$$\hat{n} = \frac{\alpha'}{c_0} n = \alpha' V \left[1 - \frac{(\alpha' V)^{2/3}}{15} \right] \tag{3.27}$$

The profile of $\hat{n}$ is shown in Figure 3.5.

3.1.2 Numerical solution

The complete equation 3.7 was solved numerically by using the MATLAB BVP (Boundary Value Problem) solver for ODEs `bvp5c` ([13]). The values assigned to the various parameters are taken from [1] and reported in Table 3.1. For what concerns boundary conditions, besides $\hat{c}(1) = 1$, requiring a non-diverging concentration in $\lambda = 0$ is actually equivalent to imposing $\hat{c}'(0) = 0$. The equation was solved for three different values of the parameter κ, namely $\kappa = 0.005, 0.025, 0.125$. A solution was obtained for 15 values of the sphere radius that were all chosen in an interval from 50 μm to 50000 μm. The graphs of B and n as a function of the volume of the sphere V are reported in Figure 3.6a and 3.6b respectively. Figure 3.7 shows the dependence of B upon n. The values of the scaling exponents for both small

Parameter	Description	Value
D	Diffusion constant of oxygen in water (300K)	3.0×10^{-9} m^2/s
k_m	Michaelis-Menten constant for hepatocytes	7.39×10^{-3} mol/m^3
v_{max}/ρ	Limiting cellular metabolic rate	4.8×10^{-17} mol/(cell·s)
ρ	Typical *in vitro* cell density	5.14×10^{12} cell/m^3

Table 3.1: Values of various parameters used for the numerical solution of equation 3.7. These correspond to the choices made in [1].

and large values of V are listed in the figure's captions. The straight lines were not plotted for the sake of clarity.

The results of the calculation are qualitatively the same found in [1], at least for what concerns the allometric scaling of the metabolic rate. B is observed to scale linearly with V for small V; for large V, the scaling exponent settles around 0.7. We observe also the same behavior for the total number of moles n: as a matter of fact, B scales following a roughly isometrical relation with n (see Figure 3.8).

The fact that the scaling exponent for B varies continuously from 1 to about 0.7 suggests (as explained in [1]) the possibility of identifying a working window for the values of the parameters β and κ in which Kleiber's law is obeyed: the metabolic rate per cell should then follow a $-1/4$ power law without the need of any vascularisation.

3.2 Different boundary conditions

As explained earlier, in order to solve equation 3.7, the choice made in [1] was to set

$$\left.\frac{\partial \hat{c}(\lambda)}{\partial \lambda}\right|_{\lambda=0} = 0 \tag{3.28}$$

This is the only possibility (at least for the analytically solvable cases) if one wants to avoid the divergence of the concentration in $\lambda = 0$. There are

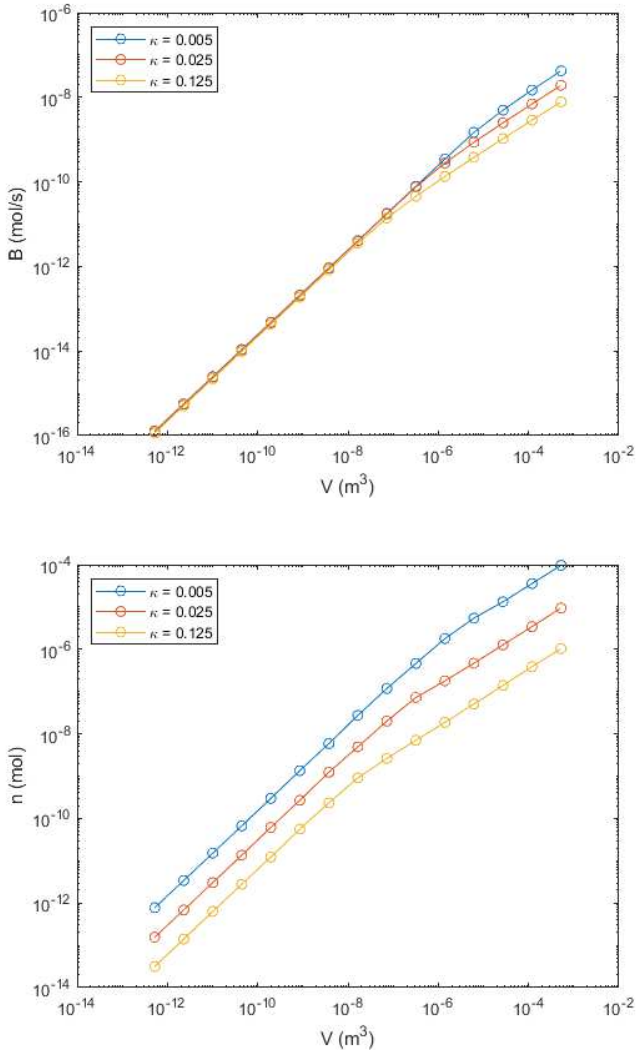

Figure 3.6: (a) B as a function of V for different κ. For small volumes, $B \sim V$ independently on the value of κ. For large volumes, the exponents are: 0.7229 ($\kappa = 0.005$), 0.6978 ($\kappa = 0.025$), 0.6802 ($\kappa = 0.125$). (b) n as a function of V for different κ. Exponents for small volumes: 1.0038 ($\kappa = 0.005$), 1.0058 ($\kappa = 0.025$), 1.0096 ($\kappa = 0.125$). Exponents for large volumes: 0.6700 ($\kappa = 0.005$), 0.6770 ($\kappa = 0.025$), 0.6800 ($\kappa = 0.125$).

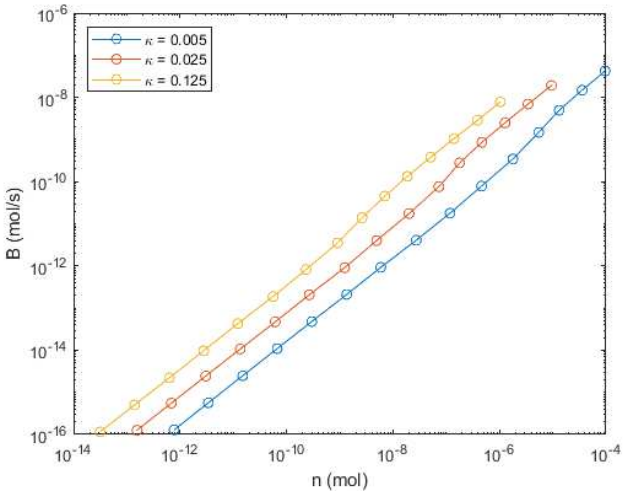

Figure 3.7: B as a function of n for three different values of the parameter κ. Exponents for small volumes: 0.9962 ($\kappa = 0.005$), 0.9942 ($\kappa = 0.025$), 0.9904 ($\kappa = 0.125$). Exponents for large volumes: 1.0577 ($\kappa = 0.005$, 1.0306 ($\kappa = 0.025$), 1.0003 ($\kappa = 0.125$).

however some issues related to this choice. Firstly, there is no apparent physical reason for which the concentration should exhibit a vanishing derivative at the origin. Secondly, even though it is true that without imposing the condition 3.28 the concentration would diverge, it is also true that it would do so as $\sim 1/\lambda$. Since in the computation of the total number of moles n the concentration $\hat{c}(\lambda)$ has to be multiplied by λ^2, the divergence would be effectively harmless: the integral would in any case stay finite.
We therefore proceeded in the following way: instead of considering the function $\hat{c}(\lambda)$, we considered $y(\lambda) = \lambda\hat{c}(\lambda)$, which ought to be finite everywhere in $[0, 1]$. Equation 3.7 becomes

$$\frac{\partial^2 y(\lambda)}{\partial \lambda^2} = \beta^2 \kappa \frac{\lambda y(\lambda)}{\kappa\lambda + y(\lambda)} \tag{3.29}$$

Equation 3.29 has the advantage that, $y(0)$ being finite, it can be solved by making $y'(0)$ an adjustable parameter to verify how B and n get modified. In terms of the function $y(\lambda)$, the boundary condition $\hat{c}(1) = 1$ simply becomes $y(1) = 1$. In terms of the function $y(\lambda)$ equations 3.8 and 3.9 become

$$B = 4\pi D c_0 R(y'(1) - 1) \tag{3.30}$$

$$n = 4\pi c_0 R^3 \int_0^1 d\lambda \lambda y(\lambda) \tag{3.31}$$

respectively. There are some constraints that have to be taken into account when trying to identify some plausible values for $y'(0)$.

- the function $y(\lambda)$ must be positive for every $\lambda \in [0, 1]$, and such that $y(1) = 1$;
- in order to have a positive metabolic rate, one needs to require that $y'(1) > 1$.

As can be noted from equation 3.29, $y(\lambda)$ is a convex function of λ, i.e. $y'(\lambda)$ increases as λ becomes larger. Thus, for example, $y'(0)$ cannot be too small, because there is the possibility that $y'(\lambda)$ does not increase enough to meet the condition $y'(1) > 1$, especially for small values of β (since the curvature is proportional to β^2). On the other hand $y'(0)$ cannot be excessively large, because this could not be in agreement with the requirement that $y(\lambda)$ is always positive and $y(1) = 1$. For these reasons, there is the need of identifying a range of values for $y'(0)$ such that all the conditions listed before are met.

In order to do that, one possibility is to look for an approximate solution by expanding the r.h.s of equation 3.29 up to first order

$$\frac{\partial^2 y(\lambda)}{\partial \lambda^2} \simeq \beta^2 \kappa \lambda \tag{3.32}$$

After integrating twice, this yields

$$y(\lambda) \simeq \frac{\beta^2 \kappa}{6} \lambda^3 + y'(0)\lambda + y(0) \tag{3.33}$$

Now this has to satisfy the condition $y(1) = 1$, thus we can fix $y(0)$

$$y(0) = 1 - \frac{\beta^2 \kappa}{6} - y'(0) \implies y(\lambda) \simeq \frac{\beta^2 \kappa}{6}(\lambda^3 - 1) + y'(0)(\lambda - 1) + 1 \tag{3.34}$$

We now require that $y'(1) > 1$ and, at the same time $y(\lambda) \geq 0 \; \forall \lambda \in [0, 1]$. This leads to

$$1 - \frac{\beta^2\kappa}{2} \leq y'(0) \leq \min_{0\leq\lambda\leq 1} \frac{1 + \frac{\beta^2\kappa}{6}(\lambda^3 - 1)}{(1-\lambda)} \tag{3.35}$$

Notice that the boundaries of the interval for the possible values of $y'(0)$ depend both on β and κ. At this point, let's call y'_{low} and y'_{up} the lower and upper boundary of equation 3.35 respectively. Figure 3.8 shows the dependence of y'_{low} and y'_{up} with respect to the quantity $\beta^2\kappa$. The numerical

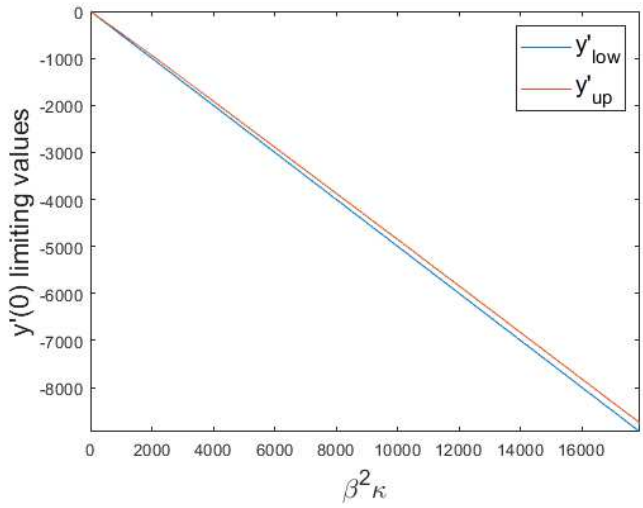

Figure 3.8: y'_{low} and y'_{up} as a function of $\beta^2\kappa$.

integration of equation 3.29 was performed for three different values of $y'(0)$, namely

$$y'(0) = y'_{low} + m\frac{y'_{up} - y'_{low}}{4} \tag{3.36}$$

with $m = 1, 2, 3$. The values of the parameters are again the ones presented in Table 3.1. The equation was solved for 15 different values of the sphere radius R varying (as before) from 50 μm to 50000 μm. Interestingly, the behavior of B does not change significantly with respect to the results of the previous section. The biggest difference is observed for n, which displays a superlinear dependence on V when this becomes large.

Also, we observe that the particular value of $y'(0)$ in the interval defined in equation 3.35 has almost unnoticeable effects on the scaling of B and n: in

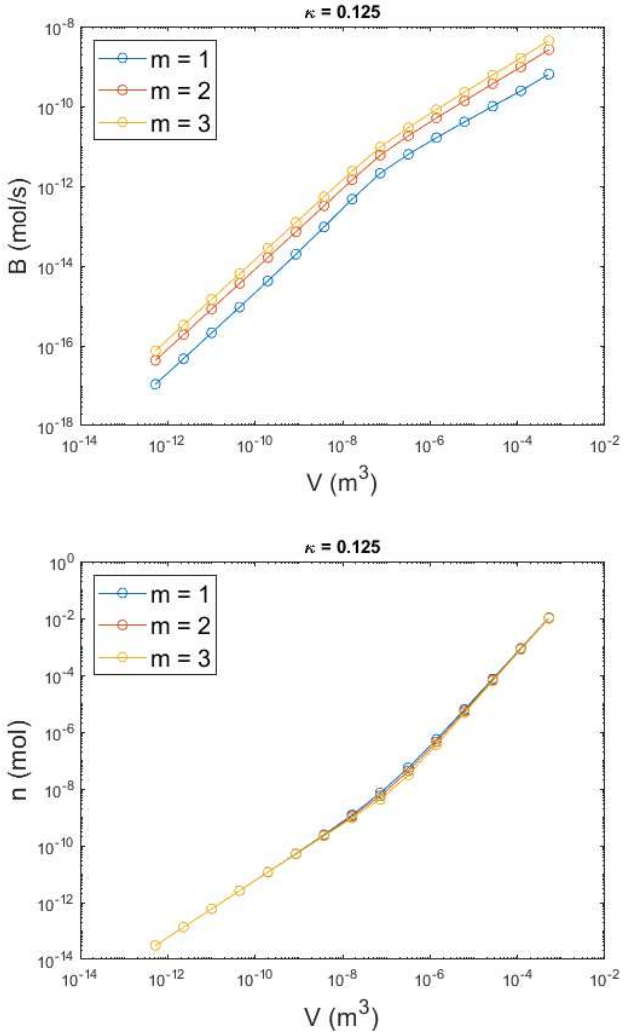

Figure 3.9: (a) B as a function of V for different values of $y'(0)$ in the interval specified in 3.35, for $\kappa = 0.125$. Exponents for small V: 1.0032 ($m = 1$), 1.0004 ($m = 2$), 1.0005 ($m = 3$). Exponents for large V: 0.6184 ($m = 1$), 0.6634 ($m = 2$), 0.6700 ($m = 3$). (b) n as a function of V for different values of $y'(0)$ in the interval specified in 3.35, for $\kappa = 0.125$. Exponents for small V: 1.0010 ($m = 1$), 1.0005 ($m = 2$), 0.9999 ($m = 3$). Exponents for large V: 1.6718 ($m = 1$), 1.6943 ($m = 2$), 1.7200 ($m = 3$).

the case of n, the three curves overlap almost perfectly. This fact is somewhat expected if one looks at Figure 3.8: for any given value of $\beta^2\kappa$, the interval identified by equation 3.35 is quite narrow.

Another possibility is to assume that the oxygen consumption is regulated by a Hill equation, which is a sort of generalized Michaelis-Menten (see Appendix B)

$$v_{max}\frac{c^n(r)}{k_m^n + c^n(r)} \tag{3.37}$$

where n is a positive integer. If $n = 1$, the Michaelis-Menten consumption is recovered. The equation was solved with the same boundary conditions for $n = 2, 3, 4$. No significant changes in the scaling of B and n have been observed.

3.2.1 Optimal κ

The most notable feature of this system is that, regardless of the particular boundary condition in $\lambda = 0$, the scaling exponent of the metabolic rate B varies continuously from 1 to 2/3.

It would be possible therefore to express the scaling exponent of the metabolic rate as a function of the volume V: actually, assuming a mass density equal to the density of water ([1]), one can check the dependence of the scaling exponent on the mass M rather than on the volume V. In order to do that, there is the need of choosing a value for $y'(0)$: since from the previous analysis no significant differences have been observed in the scaling behavior for different values of the parameter m, one can fix $m = 2$, which is equivalent to assume that $y'(0)$ lies in the middle of the interval identified in 3.35. The scaling exponent as a function of M was computed different values of κ. The result is shown in Figure 3.10.

The latter figure also highlights the fact that for every κ there exists a value of M, let's call it M^*, such that the scaling exponent is equal to 3/4, which is what we want to achieve. At this point, the scaling behavior was determined for several values of κ spacing from 10^{-2} to 10^{-1}. For each curve, the value of M^* was extrapolated. In this way, we have obtained the function $M^*(\kappa)$.

A further observation is that the latter function can be inverted, yielding $\kappa(M^*)$, which has the following physical meaning: if the spherical cell con-

struct has mass M^*, then a 3/4 power scaling metabolic rate is achieved by tuning $\kappa = \kappa(M^*)$.

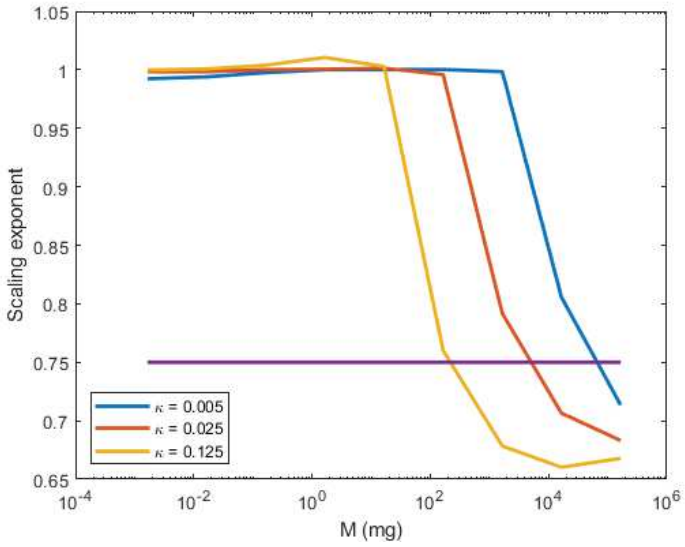

Figure 3.10: Scaling exponent of the metabolic rate as a function of the mass M of the cell construct. The results were obtained for $\kappa = 0.005, 0.025, 0.125$.

The function $\kappa(M^*)$ is presented in Figure 3.11 (left panel). Quite interestingly, the function is well fitted by a power law with an exponent of -0.575.

The same procedure was repeated following the assumptions made in [1] for the boundary conditions in $\lambda = 0$. The result is shown in Figure 3.11 (right panel). The power law behavior of $\kappa(M^*)$ is observed also in this case, even though the exponent is found to be -0.693.

3.3 Remarks

From the analysis carried out in this chapter, the presence of a crossover between different values of the scaling exponent is apparent, regardless of the boundary conditions for the concentration at the origin. This crossover behavior has been observed also in other models of actual living organisms: in [5], the authors argue that the allometric exponent for the metabolic rate

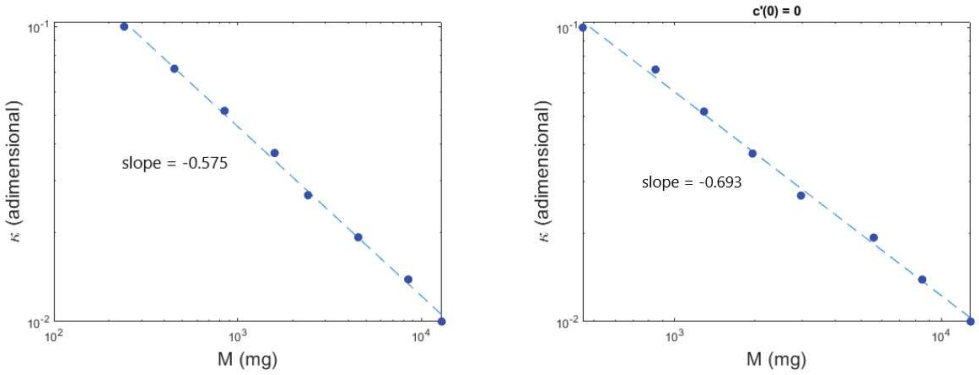

Figure 3.11: (Left panel) The function $\kappa(M^*)$ obtained by choosing $y'(0)$ as the middle point of the interval 3.35. (Right panel) The same function obtained following the hypothesis from [1] on the boundary condition in $\lambda = 0$.

changes from small to large values of the mass M, mirroring the behavior of the *in vitro* system considered here. However, the *in vitro* crossover is achieved within a much smaller range of M.

Nevertheless, it would seem possible to prepare an *in vitro* system with a 3/4 metabolic scaling by modulating the oxygen supply c_0, at least in the range for the parameters that has been taken into account. In particular, the optimal value of $c_0 = k_m/\kappa$ is an increasing function of the sphere's mass which is well fitted by a power law (assuming that the Michaelis-Menten constant does not depend on M).
Another point to be noticed is that the crossover of different scaling exponents (i.e. 1 and 2/3) does not seem to depend heavily on the particular expression for the oxygen consumption. As a matter of fact, in the various cases that have been analyzed four different forms of consumption have been utilized: linear, constant, Michaelis-Menten and Hill equation. The modification of the consumption term in equation 3.7 did not lead to significant changes in the metabolic scaling of the system. A further analysis could be focused on the dependence of the results on the diffusion term: an interesting question to be addressed is what would happen if one considers processes of super- or sub-diffusion, such that the Laplacian in equation 3.7 is modified.

Conclusions

In this work, the significance of the phenomenon known as allometric scaling has been highlighted. In particular, the central role of Kleiber's law from a biological and ecological perspective has been discussed. On one hand, we have seen how the behavior of several biological variables is ultimately a consequence of the mechanisms and the extent to which energy is exploited by an organism of a given size. Indeed, *"metabolism, like inheritance, is one of the great unifying processes in biology"* ([6]). This fact suggests the fundamental importance of Kleiber's law as a key-element for the understanding of (possibly) every other allometric scaling relation.

On the other hand, we have seen how the metabolic performances of individuals affect the structure of Life at more complex levels of organization, e.g. communities and populations. The Metabolic Theory of Ecology, which was presented in Chapter 1, provides a theoretical framework which seems able to predict the magnitudes and to shed light on the mechanisms at the core of many empirical phenomena in ecology. For example, we've seen that starting from equation 1.4 one can estimate the dependence of variables such as lifespan, developmental rates, population density and many others on body mass M and body temperature T. Also, the species richness in a given environment and the dynamics of trophic levels are explained within this framework ([6]). This theory accounts for the variation of biological and ecological quantities over a surprisingly wide range. However, significant individual variation is observed in the empirical data. The reason underlying these deviations from the predicted behavior is that the Metabolic Theory of Ecology *"is not a theory of everything"*([6]): metabolism and allometry are undoubtedly fundamental aspects of Life at all scales, but they're not the only ones. Individual variations from the expected pattern actually calls attention on the importance of other biological quantities or processes, which need to be understood in order to construct a solid unifying framework for

Ecology. The direction and magnitude of the deviations with respect to the predictions in the individual cases can become a useful starting point for the construction of a more comprehensive theory.

Along with allometry, the finite-size scaling framework (equation 2.13) has proven to be very powerful for what concerns the description of forest communities. Indeed, a power law distribution is what could be expected for systems in which quantities (e.g. tree height, trunk diameter) are distributed over such wide ranges, so that the system is lacking a typical scale. The model presented in [21] has proven successful in the identification of the scaling exponents for the distributions of several quantities; moreover, the model is able to provide a link between the various exponents. Even more importantly, the model establishes a relation between exponents that belong to two different domains through equation 2.20: the exponent H is related to the shape of an individual tree and its metabolic efficiency, whereas α is related to the entire forest, because it determines the form of the height distribution. This is another example which supports Metabolic Theory and its efficacy.

The importance of a detailed knowledge of the structure of forest communities has already been mentioned: forests are vital for our planet because of the CO_2 consumption and O_2 production: being able to quantify for instance the net amount of carbon dioxide consumed by a forest in a given period (which is proportional to the total metabolic rate of the forest) can bring significant suggestions in the planning of anthropogenic activity, and consequently to global economy. From this side, being able to model also *dynamical* forests would be very meaningful (recall that the model in [21] deals with steady-state forests): further theoretical work could be focused on how the distribution of a certain quantity y, i.e. $p_y(y|y_c)$, changes with time when the system starts from a given initial configuration.

In Chapter 3 we have seen how the role of allometry is not restricted to natural systems, but it can be a useful framework for experimental work. Kleiber's law seems so intrinsically related to life that researchers were led to attempt to reproduce it in an *in vitro* environment, in order to be able to mimic the functioning of an actual organism. The fact that cells in *in vitro* cultures do not obey Kleiber's law suggests however that the 3/4 (or -1/4) power scaling does not come built in cells: it must be something that belong to a higher level of organization that gives rise to the behavior that is empirically observed. This is why the various theoretical models that have attempted to explain Kleiber's law up to now have all focused on the distribu-

tion network rather than on the functioning of individual cells. Nevertheless, the results obtained in the last chapter suggest that it ought to be possible to reproduce the 3/4 power scaling by modifying the oxygen supply to the cell construct according to the mass of the construct itself: interestingly, the oxygen supply must increase sublinearly with the culture's mass following a power law. The exponent of such power law is different when one considers different boundary conditions at the origin for the oxygen concentration inside the sphere.
Despite the fact that this model was conceived for *in vitro* systems, it still has some translational power to actual living organisms: it could be argued that the terminal units of the resources distribution network provide nourishment to a given volume of metabolically active tissue by maintaining a constant oxygen concentration at the surface of such volume. Oxygen thus diffuses inside the volume and its consumption is regulated by a Michaelis-Menten formula (or maybe by the Hill equation, since no differences in the results have been observed between these two). The oxygen concentration is such that the metabolic rate of a single service volume is proportional to the tissue mass to the power 3/4. Since the mass of the whole organism is proportional to the mass of the service volumes, Kleiber's law would be recovered.

Unfortunately, we still lack a comprehensive mathematical model that is able to provide a theoretical foundation to Kleiber's law, which validation is still mostly empirical. Understanding the true origin of the quarter power scaling in allometry would mean a lot from both a practical and theoretical point of view. A detailed knowledge of this phenomenon could imply a higher precision in the determination of the scaling exponent (also accounting for deviations from the expected quarter power scaling) and thus more accurate predictions about ecological quantities would be possible. From a theoretical perspective, explaining Kleiber's law (and allometric scaling in general) would mean to become aware of a new basic, fundamental principle of Life which is shared by all living organisms despite their astounding diversity and complexity.

Appendix A

In this appendix an analytical derivation of the distribution of the range of influence in a random scenario is provided (see Section 2.2.3). Suppose we have a d-dimensional volume V in which N points are uniformly distributed at random positions. We assign to each point a random number picked from a distribution p. Let's define

$$P_{>}(x) = \int_{x}^{+\infty} dz p(z) \tag{A.1}$$

which is the probability that the random number associated to a point is greater than a certain value x. The density of such points, denoted by $\rho_{>}(x)$, is given by

$$\rho_{>}(x) = P_{>}(x)\frac{N}{V} \tag{A.2}$$

The typical volume of a region containing only one of these points, indicated with $v_{>}(x)$, satisfies

$$v_{>}(x)\rho_{>}(x) \approx 1 \tag{A.3}$$

It follows that the linear size of such volume, which coincides with the typical range of influence as defined in section 2.2.3, is approximately equal to $(\rho_{>}(x))^{-1/d}$. Thus it is possible to determine the distribution of the range of influence p_{r_i} as

$$p_{r_i}(r_i) = \int_{-\infty}^{+\infty} dx p(x)\delta(r_i - \rho_{>}^{-1/d}(x)) \tag{A.4}$$

where δ is the Dirac delta function. One property of the latter is that, if x_k $(k = 1, \ldots, n)$ are the zeros of a function $f(x)$ such that $f'(x_i) \neq 0$ for every k, then the following equality holds

$$\delta(f(x)) = \sum_{k=1}^{n} \frac{\delta(x - x_k)}{|f'(x_k)|} \tag{A.5}$$

If we call $x(r_i)$ the solution of the equation $r_i - \rho_>^{-1/d}(x) = 0$, by using property A.5 we have

$$\delta(r_i - \rho_>^{-1/d}(x)) = \frac{\delta(x - x(r_i))}{\left|\frac{d}{dx}\rho_>^{-1/d}(x(r_i))\right|} = d\rho_>^{(d+1)/d}(x(r_i))\frac{\delta(x - x(r_i))}{\left|\frac{d}{dx}\rho_>(x(r_i))\right|} \tag{A.6}$$

Now $x(r_i)$ can equivalently be thought of as the solution of the equation $r_i^{-d} - \rho_>(x) = 0$. Thus we can again use property A.5 to obtain

$$\delta(r_i - \rho_>^{-1/d}(x)) = d\rho_>^{\frac{d+1}{d}}(x(r_i))\delta(r_i^{-d} - \rho_>(x)) \tag{A.7}$$

Given the definition of $x(r_i)$, we have that $\rho_>^{\frac{d+1}{d}}(x(r_i)) = r_i^{-d-1}$. Thus one finally gets

$$\delta(r_i - \rho_>^{-1/d}(x)) = dr_i^{-d-1}\delta(r_i^{-d} - \rho_>(x)) \tag{A.8}$$

At this point one can write

$$p_{r_i}(r_i) = \frac{d}{r_i^{d+1}} \int_{-\infty}^{+\infty} dx p(x)\delta(r_i^{-d} - \rho_>(x)) \tag{A.9}$$

Given the definition of the cumulative distribution $P_>(x)$ we have that

$$-\frac{d}{dx}P_>(x) = p(x) \tag{A.10}$$

By recalling the definition of $\rho_>(x)$ one obtains

$$p_{r_i}(r_i) = -\frac{V}{N}\frac{d}{r_i^{d+1}} \int_{-\infty}^{+\infty} dx \frac{d}{dx}P_>(x)\delta\left(P_>(x) - \frac{V}{N}r_i^{-d}\right) \tag{A.11}$$

With the change of variables $z = P_>(x)$ we get

$$-\frac{V}{N}\frac{d}{r_i^{d+1}} \int_1^0 dz\delta\left(z - \frac{V}{Nr_i^d}\right) = \frac{V}{N}\frac{d}{r_i^{d+1}} \int_0^1 dz\delta\left(z - \frac{V}{Nr_i^d}\right) \tag{A.12}$$

The integral in the last equality can be easily computed by noticing that, given the properties of the delta function, if $0 \leq V/Nr_i^d \leq 1$ the integral gives 1, otherwise it gives 0. This result can be summarized as

$$p_{r_i}(r_i) = \frac{V}{N}\frac{d}{r_i^{d+1}}\theta\left(r_i - \left(\frac{V}{N}\right)^{1/d}\right) \tag{A.13}$$

where θ indicates the Heaviside step function. From A.13 it immediately follows that the cumulative distribution function $P^{>}_{r_i}(r_i)$ is

$$P^{>}_{r_i}(r_i) = \int_{r_i}^{+\infty} dx p_{r_i}(x) = \begin{cases} 1 & \text{if } r_i \leq \left(\frac{V}{N}\right)^{1/d} \\ \frac{V}{N} r_i^{-d} & \text{otherwise} \end{cases} \tag{A.14}$$

The case of forests studied in section 2.2.3 is characterized by $d = 2$, and this yields $P^{>}_{r_i}(r_i) \sim r_i^{-2}$. Notice that the result does not depend on the particular form of the distribution p.

Appendix B

Enzymatic processes can schematically be summed up by the following two-stage reaction

$$E + S \underset{k_{off}}{\overset{k_{on}}{\rightleftharpoons}} ES \overset{k_{cat}}{\rightarrow} E + P \tag{B.1}$$

where E denotes the enzyme, S denotes the substrate and P is the product of the reaction. When an enzyme is bound to a substrate, an enzyme-substrate compound (ES) is created, and this happens at a rate per unit concentration k_{on}. After ES is formed, through the process of catalysis this will give the product of the reaction P and release the free enzyme E at a rate k_{cat}. ES can also decompose to $E + S$ at a rate k_{off}. Therefore, by indicating with squared parenthesis the concentrations of all the involved quantities we have the differential equation

$$\frac{d[ES]}{dt} = k_{on}[E][S] - (k_{off} + k_{cat})[ES] \tag{B.2}$$

In stationary conditions, the following relation holds

$$\frac{[E][S]}{[ES]} = \frac{k_{off} + k_{cat}}{k_{on}} = k_m \tag{B.3}$$

where we have defined the Michaelis-Menten constant k_m. The total concentration of the enzyme $[E]_{tot}$ is given by

$$[E]_{tot} = [E] + [ES] \tag{B.4}$$

Therefore one finds

$$[ES] = \frac{([E]_{tot} - [ES])[S]}{k_m} = \frac{[S][E]_{tot}}{k_m} - \frac{[ES][S]}{k_m} \tag{B.5}$$

after some simple manipulations, one obtains

$$[ES] = \frac{[S][E]_{tot}}{k_m + [S]} \tag{B.6}$$

Now the production rate of the product P, denoted with v, is simply given by $k_{cat}[ES]$. If we define $v_{max} = k_{cat}[E]_{tot}$ then we finally obtain the Michaelis-Menten formula

$$v = \frac{v_{max}[S]}{k_m + [S]} \tag{B.7}$$

This equation has the peculiar feature that it predicts the *saturation* of the reaction rate v, which is an almost universally observed behavior for enzyme (and also non-enzyme) kinetics.

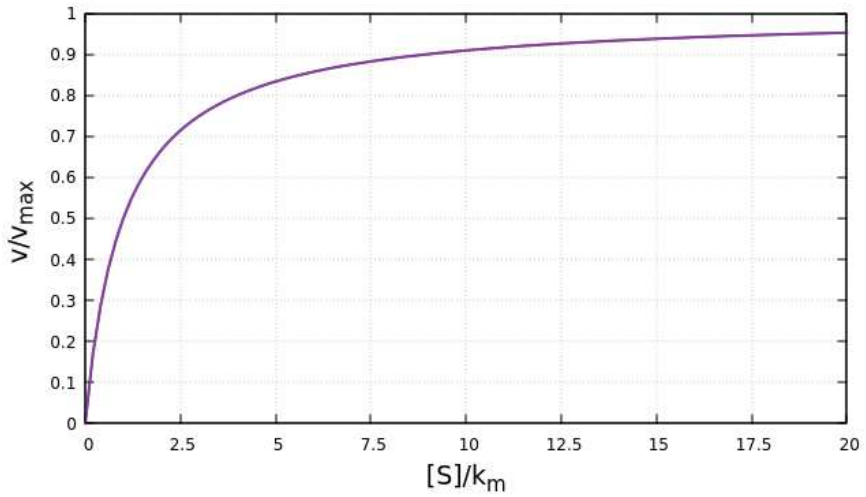

Figure B1: The quantity v/v_{max} is plotted against $[S]/k_m$ as predicted by the Michaelis-Menten formula. It is apparent how v/v_{max} scales linearly when $[S]/k_m \ll 1$, whereas it asymptotically tends to 1 for $[S]/k_m \gg 1$.

In the particular context of oxygen consumption in the model presented in [1], assuming a Michaelis-Menten kinetics implies that cells do not consume all the oxygen at their disposal: when the oxygen concentration is considerably larger than the Michaelis-Menten constant, even if the concentration varies it does not lead to significant changes in the reaction rate.

A more general formula for enzyme kinetics is given by the *Hill equation*, which can be thought of as a generalization of B.7

$$v = \frac{v_{max}[S]^n}{k_m^n + [S]^n} \tag{B.8}$$

where n is a positive integer.

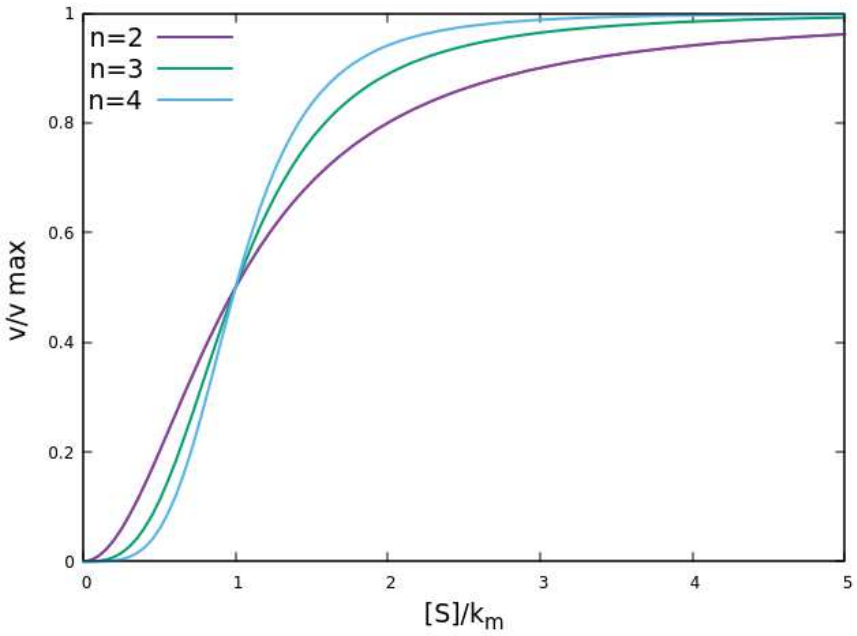

Figure B2: v/v_{max} against $[S]/k_m$ as predicted by equation B.8. Unlike equation B.7, the Hill equation does not predict a linear relation between these two quantities when $[S] \ll k_m$. However, the saturation for large values of $[S]$ is still present. Also, the saturation is achieved with smaller and smaller values of $[S]/k_m$ as n increases.

Bibliography

[1] Ahluwalia A. (2017), *Allometric scaling in-vitro*. Scientific Reports, 7, 42113.

[2] Allen A.P., Brown J.H., Gillooly J.F. (2002), *Global biodiversity, biochemical kinetics, and the energetic-equivalence rule*. Science, 297:1545-1548

[3] Anfodillo T., Carrer M., Simini F., Popa I., Banavar J.R., Maritan A. (2013), *An allometry-based approach for understanding forest structure, predicting tree-size distribution and assessing the degree of disturbance*. Proceedings of the Royal Society B:Biological Sciences, 280(1751):20122375.

[4] Banavar J.R., Maritan A., Rinaldo A. (1999), *Size and forms in efficient transportation networks*. Nature, 399:130-132.

[5] Banavar J.R., Cooke T.J., Rinaldo A., Maritan A. (2014), *Form, function and evolution of living organisms*. Proceedings of the National Academy of Sciences, 111(9):3332-3337.

[6] Brown J.H., Gillooly J.F., Allen A.P., Savage V.M., West G.B. (2004), *Toward a metabolic theory of ecology*. Ecology, 85:1771-1789.

[7] Damuth J. (1981), *Population density and body size in mammals*. Nature, 290(5808):699-700.

[8] Gillooly J.F., Brown J.H., West G.B., Savage V.M., Charnov E.L. (2001), *Effects of size and temperature on metabolic rate*. Science, 293:2248-2251.

[9] Gillooly J.F., Charnov E.L., West G.B., Savage V.M, Brown J.H. (2002), *Effects of size and temperature on developmental time*. Nature 417:70-73.

[10] Houghton R.A. (2007), *Balancing the global carbon budget*. Annu. Rev. Earth Planet. Sci., 35:313-347.

[11] Hulbert A.J. (2014), *A sceptics view:"Kleiber's law" or the "3/4 rule" is neither a law nor a rule but rather an empirical approximation*. Systems, 2:186-202.

[12] Huxley J.S., Teissier G. (1936), *Terminology of relative growth*. Nature, 137(3471):780-781.

[13] Kierzenka J., Shampine L.F. (2007), *A BVP solver that controls residual and error*. JNAIAM J. Numer. Anal. Ind. Appl. Math, 3(1-2):27-41.

[14] Kleiber M. (1932), *Body size and metabolism*. Hilgardia, 6:315-353.

[15] Kozlowski J., Konarzewski M. (2004), *Is West, Brown and Enquist's model of allometric scaling mathematically correct and biologically relevant?* Functional Ecology, 18(2):283-289.

[16] Livi R., Politi M., (2017), *Nonequilibrium statistical physics: a modern perspective*. Cambridge University Press.

[17] Miller G.A. (1957), *Some effects of intermittent silence*. The American Journal of Psychology, 70(2):311-314.

[18] Moraes C., Labuz J.M., Leung B.M., Inoue M., Chun T.H., Takayama S. (2013), *On being the right size: scaling effects in designing human-on-a-chip*. Integrative Biology, 5(9):1149-1161.

[19] Munoz M.A. (2018), *Colloquium: Criticality and dynamical scaling in living systems*. Reviews of Modern Physics, 90(3):031001

[20] Newman M.E.J. (2005), *Power laws, Pareto distributions and Zipf's law*. Contemporary Physics, 46(5):323-351.

[21] Simini F., Anfodillo T., Carrer M., Banavar J. R., Maritan A. (2010), *Self-similarity and scaling in forest communities*. Proceedings of the National Academy of Sciences, 107(17):7658-7662.

[22] Vozzi F., Heinrich J.M., Bader A., Ahluwalia D.A. (2009), *Connected culture of murine hepatocytes and human umbilical vein endothelial cells in a multicompartmental bioreactor*. Tissue Engineering Part A, 15(6):1291-1299.

[23] West G.B., Brown J.H., Enquist B.J. (1997), *A general model for the origin of allometric scaling laws in biology*. Science, 276:122-126.

[24] West G.B., Brown J.H., Enquist B.J. (2001), *A general model for ontogenetic growth*. Nature, 413:628-631.

[25] West G.B., Woodruff W.H., Brown J.H. (2002), *Allometric scaling of metabolic rate from molecules and mitochondria to cells and mammals*. Proceedings of the National Academy of Sciences, 99(1):2473-2478.

[26] Zaoli S., Giometto A., Maritan A., Rinaldo A. (2017), *Covariations in ecological scaling laws fostered by community dynamics*. Proceedings of the National Academy of Sciences, 114(40):10672-10677.